Journal Pre-proof

Kinetic investigation of eggshell powders as biobased epoxy catalyzer

Nichollas Guimarães Jaques, José William de Lima Souza, Matthias Popp, Jana Kolbe, Marcus Vinícius Lia Fook, Renate Maria Ramos Wellen

PII: S1359-8368(19)33408-0

DOI: https://doi.org/10.1016/j.compositesb.2019.107651

Reference: JCOMB 107651

To appear in: *Composites Part B*

Received Date: 16 July 2019

Revised Date: 28 October 2019

Accepted Date: 28 November 2019

Please cite this article as: Jaques NichollasGuimarã, William de Lima Souza José, Popp M, Kolbe J, Lia Fook MarcusViní, Ramos Wellen RM, Kinetic investigation of eggshell powders as biobased epoxy catalyzer, *Composites Part B* (2020), doi: https://doi.org/10.1016/j.compositesb.2019.107651.

Kinetic investigation of eggshell powders as biobased epoxy catalyzer

Nichollas Guimarães Jaques [1], José William de Lima Souza [1], Matthias Popp [2], Jana Kolbe [2], Marcus Vinícius Lia Fook [1] and Renate Maria Ramos Wellen* [1,3]

[1] *Academic Unit of Materials Engineering, Federal University of Campina Grande, Campina Grande 58249-140, Brazil;*

[2] *Fraunhofer-Institut für Fertigungstechnik und Angewandte Materialforschung (IFAM), Wiener Straße 12, D-28359 Bremen, Germany;*

[3] *Materials Engineering Department, Federal University of Paraiba, João Pessoa 58051-900, Brazil*

** Correspondence: wellen.renate@gmail.com*

Abstract

Epoxy resins from bisphenol A of diglycidyl ether / anhydride methyl tetrahydrophthalic / 2,4,6-tris dimethylaminomethyl phenol were prepared by mechanical mixing using a magnetic stirrer. Substitution of synthetic catalyzer by eggshell powders provided high performance biobased materials. Chemical character analysis of epoxy/eggshell carried out using dispersive energy spectrometry, and Fourier transform infrared spectroscopy, acquired data indicated the eggshell membrane as a suitable catalyzer for the cross-linking reaction, due to the presence of amines, hydroxyl and sulphur that could participate in the cross-link reaction. The cure kinetics was investigated using differential scanning calorimetry and applying Ozawa, Kissinger, Friedman isoconversional, Málek, and Friedman model-based, where Málek and Friedman model-based presented the best fits to describe synthetic and biobased materials.

Keywords: Epoxy, chicken eggshell powder, cure kinetics.

1. Introduction

Epoxies are thermosets with wide application for several industrial branches, such as electronics, aerospace, automotive and biomaterials; due to their properties such as chemical, mechanical and thermal resistance, adhesiveness, dimensional stability and electrical insulation; they are used in high quality and long-lived products. Nevertheless, the epoxy resin commonly used in the industry made from the precursor diglycidyl ether of bisphenol A (DGEBA), has a fragile character, with low impact strength, long cross-linking times, together with non-biodegradable character, therefore improvements fulfilling these lacks would be welcome scientific and technological advances to both academy and industry [1–3].

In order to figure out such restrictions, fillers have been added to these polymers, as barium ferrite, graphene, graphite oxide, multiwalled carbon nanotubes, alumoxane [4–8], however drawbacks such as high costs, agglomeration and complex processing along with growing concern focus at development of sustainable materials have directed researchers to seek for alternative materials, made from natural sources [9–11].

Among natural reinforcements, chicken eggshell has been an attractive option, due to its low cost, good thermal and mechanical resistance [9, 12, 13]. In Brazil, annually 16.000 tons of eggshell are discarded, being considered one of the food industry byproducts, which brings environmental impacts [14]. Therefore, the reuse of this waste becomes essential. Also, its nanoporous surface and presence of reactive functional groups such as sulfur, amines, carboxylic acids may act as interaction bridges with epoxy promoting its curing and mechanical performance [15].

In general, epoxy resins have high reactivity due to the unstable state of twisted oxirane rings. Thus, even though the curing reaction is predominantly controlled by hardener and catalyzer present in the system, dispersed loads in the matrix, such as eggshell powder, may act positively accelerating the curing process [2, 3, 16]. Because of the complex epoxy cross-linking reactions, control of the processing and composition conditions to achieve the final designed properties has become a challenge. Consequently, the kinetic study of the cure reactions become an essential tool for a more effective control of the process parameters.

Saeb et al [13] performed the kinetic study of epoxy cure with synthetic calcium carbonate ($CaCO_3$) and eggshell powder. The effect of surface modification of these particles was also evaluated. Applying Friedman and Málek models the epoxy and epoxy/eggshell cure reactions wwere observed to follow an autocatalytic type, which was corroborated by the sum of reaction orders (n + m) with values higher than 1. From Friedman isoconversional model, it was verified higher levels of eggshell without superficial modification presented lower activation energy (E_a), suggesting this filler made easier the curing process. The fit deviation between theoretical and experimental data was verified most due to measured activation energy as the maximum peak height not representing the reaction as a whole.

Mustata et al. [17] searched the thermal behavior of epoxy with ($CaCO_3$) from Rapana thomasiana shells. From Ozawa and Kissinger models, E_a and pre-exponential factor (A) were determined. The authors observed a decrease in both kinetic parameters increasing $CaCO_3$ content, evidence of less perfect lattice networks was also verified.

In a previous work conducted by our group [18], the feasibility of using chicken eggshell powder as a catalyzer substitute during the cure of bisphenol A diglycidyl ether (DGEBA) was evaluated. Between the two main structures of the eggshell, i.e., the shell composed mainly by $CaCO_3$, and the membrane composed by proteins and carbohydrates, the membrane showed to be a better cure catalyzer, making it faster and in lower temperatures. Additionally, greater tensile strength and higher deformation were reached, translating in an attractive alternative for the development of sustainable and protective environment materials. Based on the aforementioned, deeper investigation focused at cure kinetics of DGEBA added with egg membrane (M) will provide properly tools to the better understanding of cure parameters.

This work aims to study the cure kinetics of DGEBA/MTHPA upon addition of eggshell (E), or membrane (M) powders compounds; five heating rates ranging from 1 to 20 °C/min carried out using differential scanning calorimeter (DSC) and Ozawa, Kissinger, Friedman and Málek models were applied to evaluate the kinetic parameters. Besides, the chemical structure developed before and after curing was investigated using dispersive energy spectroscopy (EDS) and fourier transform infrared spectroscopy (FTIR).

2. Materials and Methods

2.1. Materials

Bisphenol A diglycidyl ether (DER 331) with epoxide equivalent weight of 182–192 g/eq, anhydride methyl tetrahydrophthalic (MTHPA) and 2,4,6-tris(dimethylaminomethyl)phenol (DEH 35) were supplied by Olin Corporation (São Paulo, Brazil). Chicken eggshell (E) was supplied by a local farm (Campina Grande-PB, Brazil).

2.2. Methods

2.2.1. Eggshell powder treatment

Processing of eggshell powder (E) and membrane (M) was performed as an adaptation of methodology proposed elsewhere [18]. E was washed in sodium hypochlorite (NaClO) and afterward immersed in water for 2 h to remove the membrane. E and M were dried in an oven at 100 °C for 24 h. Both materials were ground in a coffee mill B55 Botini (Bilac, SP, Brazil) and sieved through #325 and #200 mesh, respectively.

2.2.2. Sample preparation

Epoxy compounding at 100:87 (DER 331/MTHPA/resin/hardener) with DEH 35 at concentrations 0, 1, 2, and 5 pcr (parts per hundred) were mixed in a magnetic stirrer for 5 min at 800 rpm.

E and M in contents of 5 and 10 pcr were added into 100:87 (DER 331/MTHPA). Afterwards, these compounds were mixed in a magnetic stirrer from Corning (Reynosa, Mexico) for 5 min at 800 rpm at ambient temperature (23 $^{\circ}$C). Compounds produced in this work are coded as presented in Table 1.

2.2.3. Chemical analysis applying fourier transform infrared spectroscopy (FTIR) and dispersive energy spectroscopy (EDS)

FTIR analysis in attenuated total reflectance (ATR) mode was performed in 4000-600 cm^{-1} wavelength range, with 16 scans and 4 cm^{-1} resolution. The equipment used was Perkin Elmer Spectrum 400 (Waltham, Massachusetts, USA), and data modeling was done in Spectrum software. This analysis was performed in selected compositions before and after curing, as presented in Table 2, where temperature profile used to produce sample tests for tensile experiments are also presented.

E and M neat powders, as well as sample tests produced with them, were submitted to EDS analysis using backscattered electrons from scanning electron microscope (SEM) World Phenom Pro X800-08334 (Eindhoven, The Netherlands).

2.2.4. Cure kinetic measurements

The curing process was analyzed by differential scanning calorimetry (DSC), using a DSC Q20 from TA Instruments (New Castle, DE, USA). Samples of approximately 5 mg were tested in a standard closed aluminum pan, under a nitrogen gas flow of 50 mL/min. The samples were heated from 30 to 400 $^{\circ}$C, at heating rates of 1, 2, 5, 10, and 20 $^{\circ}$C/min.

For a deeper understanding of epoxy non-isothermal cure kinetics, one should take into account the beginning of reaction conversion, α = 0, which is characterized by the resin in the viscous-fluid state until it reaches the solid state, i.e., α = 1, that is the end of the polymerization/cross-linking reaction. The degree of conversion can be computed through the integration of DSC exothermic peak, i.e., the ratio between the peak in a given temperature range Δ T and the entire peak event, as described in Equation 1 [19].

$$\alpha = \frac{\int_{T_0}^{T} \mathrm{H}_T}{\int_{T_0}^{T_\infty} \mathrm{H}_\infty} \quad (1)$$

The rate at which the reaction occurs is dictated by the function of conversion rate as shown in Equation 2, which is reactant availability dependent [f (α)], and the cure temperature [k (T)]. In which k (T) is characterized by Arrhenius function, Equation 3, and f (α) by the reaction mechanism function [19].

$$\frac{d\alpha}{dt} = k\ T\ \ f\ \ \alpha \quad (2)$$

$$k\ T\ = A exp\left(-\frac{E_a}{RT}\right) \quad (3)$$

Where, A is the pre-exponential factor, i.e., the collision among molecules of reactive functional groups; E_a the activation energy (kJ.mol^{-1}); R the universal gas constant (JK^{-1}.mol^{-1}) and T the experiment temperature (K).

In epoxy resins, predominantly, two reaction mechanisms take place: the autocatalytic reaction (Sestak-Bergren), Equation 4, or n-order, Equation 5 [13]. The n-order reactions are described by slow downing processes, in which the maximum conversion rate is reached at initial moments of reaction [20]. On the other hand, the autocatalytic reactions are characterized by acceleration of reactive functional groups at reaction beginning, promoting an autocatalysis effect, reaching a maximum point in a conversion range between 0.2-0.4 [13, 21]. Depending on the system, the

conversion range, and the thermal profile analyzed, the cure reaction can proceed by a single mechanism or both concomitantly.

$$f(\alpha) = \alpha^{m}(1-\alpha)^{n} \quad (4)$$

$$f(\alpha) = (1-\alpha)^{n} \quad (5)$$

Where m and n are reaction orders; autocatalytic and order n, respectively. Since (m + n) is the total order reaction.

In general, the appropriate reaction mechanism choice for applying the kinetic cure models is difficult due to the cure complexity as well as the measurement of active, reactive groups. Based on this, isoconversional models are employed using boundary conditions in which the reaction mechanism is not wholly determined, using constant conversion rates. The isoconversional models can be obtained by integrating methods (Ozawa and Kissinger), derivation (Friedman), and incrementing one (Vyazovkin) [22, 23]. In this work, Ozawa, Kissinger, and Friedman methods are applied.

Ozawa model considers E_a constant throughout the conversion range. Also, the maximum reaction rate - at the peak temperature (T_p) - is independent of the heating rate (β). In this model, the activation energy is determined by non-isothermal scans at different heating rates, from the linear regression of log β versus 1000/T_p, Equation 6, where E_a corresponds to the linear equation slope and ln [Af (α)] its intercept [24].

$$\frac{d\ln\beta}{d\left(\frac{1}{T_p}\right)} = \frac{-1{,}502\,E_a}{R} \quad (6)$$

Similarly, the Kissinger model provides the activation energy at a given constant conversion point. From non-isothermal scans, the linear regression of versus 1000/T_p, computing E_a, and the pre-exponential factor A by the intercept and slope of the plot, according to Equation 7 [25].

$$\frac{d\left(\ln\frac{\beta}{T_p^2}\right)}{d\left(\frac{1}{T_p}\right)} = \frac{-E_a}{R} \quad (7)$$

In contrast to the two previous models, in Friedman, both kinetic parameters E_a and ln [Af (α)] dependent on the reaction conversion rate, thus E_a is not assumed constant [19]. In the cure reaction, there is an increase in the viscosity and decrease of reactive functional groups, changing these parameters. Additionally, the Friedman model is limited to the evaluation of cure processes, which are governed by more than one E_a, i.e., reactions are simultaneously controlled by more than one mechanism. Generally, this happens in the final stages of the epoxy cure reaction, where diffusion processes can control the reaction, with deviations from the fit evaluated by Friedman model [13, 26]. From linear regressions performed at several conversion points, measurement of E_a and ln [Af (α)] through slope and intercept of the plot, using Equation 8. Afterwards, polynomial functions are evaluated to identify trends [19].

$$\ln\left(\frac{d\alpha}{dt}\right) = \ln[Af(\alpha)] - \frac{E_a}{RT} \quad (8)$$

Despite advantages of isoconversional models, some limitations are verified: (1) adoption of global E_a for the whole reactions, failing to describe systems which have changeable E_a in function of conversion, as assumed in Ozawa and Kissinger models; (2) evaluation of E_a in systems with competitive reactions. In these cases, the use of the model-based kinetic equations is advisable.

Montserrat et al. [27] proposed a model (Málek model) that defines the appropriate reaction mechanism, its kinetic parameters, as the conversion reaction for the system under analysis, the from plot profiles of Z (α) versus α and y (α) versus α – Equation 9 and 10 – and their maximum points, α_p and α_m, respectively [28].

$$Z\ \alpha = \left(\frac{d\alpha}{dt}\right)_{\alpha} T_{\alpha} \left[\frac{\pi\left(\frac{E_a}{RT_{\alpha}}\right)}{\beta}\right] \qquad (9)$$

$$Y\ \alpha = \left(\frac{d\alpha}{dt}\right)_{\alpha} \exp\left(\frac{E_a}{RT_{\alpha}}\right) \qquad (10)$$

$$\pi\ x = \frac{x^3 + 18x^2 + 88x + 96}{x^4 + 20x^3 + 120x^2 + 240x + 120} \qquad (11)$$

In which T_α is the temperature at a given degree of conversion and $\pi\left(\frac{E_a}{RT_{\alpha}}\right)$ was determined by Senum and Yang [29] using numerical methods of 4^{th} order from $\frac{d\alpha}{f\ \alpha}$ integration.

In non-isothermal studies of epoxy resins, Z (α) and Y (α) functions result in concave pattern plots, with parameters following the criterion $0 < \alpha_m < \alpha_p \neq 0.632$ characterizing an autocatalytic reaction [27, 28]. Therefore, given that p = $\frac{m}{n}$ = $\frac{\alpha_m}{1-\alpha_m}$ by the natural logarithm of Equations 2, 3 and 4:

$$\ln\left(\frac{d\alpha}{dt} e^{\frac{E_a}{RT}}\right) = \ln A + n[\alpha^p\ 1-\alpha\ ] \qquad (12)$$

Through $\ln\left(\frac{d\alpha}{dt} e^{\frac{E_a}{RT}}\right)$ *versus* $[\alpha^p\ 1-\alpha\ ]$ plot *ln* A is determined by the intercept, and n by its angular coefficient. Parameter m can be evaluated using *m = n*p*.

In the study of thermosetting resins cure, it is possible to estimate by Friedman's model the mechanism of system reaction from the linearity ln [Af(α)] versus (1 – α), Equation 13, in which its angular coefficient is associated with the coefficient of order n. However, in autocatalytic reactions, the straight line does not follow a completely linear profile with an inflection point ranging from -0.51 to -0.22, corresponding to the conversion range of 0.2-0.4. In these cases, literature reports that threefold kinetic parameters [ln A, (n + m), E_a] can be calculated by multiple linear regression, least squares or numerical computations [13, 21, 26, 30–32].

$$\ln\ Af\ \alpha = \ln\left(\frac{d\alpha}{dt}\right) + \frac{E_a}{RT} = \ln A + n\ln\ 1-\alpha \qquad (13)$$

In this present work, the aforementioned models were used during the investigation of cure kinetics in epoxy resin and epoxy/M composites.

3. Results and Discussion

3.1. Chemical analysis by EDS

The chemical interactions between fillers and epoxy resin may be better understood through elemental quantification of their main components, EDS is a proper tool to evaluate them as presented in Table 3, which data were evaluated from micrographs in Figure 1 for (a) E, (b) M, (c) S_5, (d) E_{10}, (e) EM_{10} e (f) M_{10}. According to these images, E has particulate shape whereas M is fibrous, from fractured surfaces (c) to (f) images (d) and (f), i.e., E_{10} and M_{10} presented rougher surfaces than S_5 characterizing ductile fracture with more energy absorption, corroborating the better tensile performance as seen in a previous work [18].

Through EDS it was verified, the eggshell powder has oxygen (O), calcium (Ca), nitrogen (N) and carbon (C), due to its major content of calcium carbonate ($CaCO_3$), nitrogen is present in the inter-crystalline proteins responsible for the mineralization of ceramic phase. These elements are also observed in E_{10} and EM_{10} systems. For the membrane composition, in addition to carbon and oxygen, the presence of higher nitrogen content was observed, and additionally sulfur, where these elements could constitute reactive functional groups which participate in curing reaction. Therefore, this could be an indication that the cross-linking is more favorable in membrane systems [18, 15].

3.2. Chemical analysis by FTIR

Figure 2 presents FTIR spectra of epoxy and epoxy/eggshell strucutres, before and after curing, in supplementary material the readers will find FTIR spectra of E, EM and M. These spectra were gathered in order to investigate the effectiveness of cross-linking process, since both fillers have sulfur and nitrogen, which may improve cure performance. In all compositions prior to cross-linking, absorption bands associated to the bonding vibrations of MTHPA were identified in the bands 2942 (-CH stretching), 2872 (-CH_3 stretching), 1862 (symmetrical axial deformation of -C=O), 1777 (asymmetric axial deformation of -C=O), 1469 (symmetrical angular deformation of -CH_2), 908 (deformation of the RC substituent group on cyclic anhydrides) cm^{-1} [33, 34]. For DGEBA resin the characteristic bands 3056 (oxirane ring -CH stretching), 2972 (-CH stretching), 2926 (-CH_2 stretching), 2872 (-CH_3 stretching), 1608 (stretching of C=C on aromatic ring), 1509 (C-C elongation of aromatic ring), 1132 (C-O-C elongation), 915 (oxirane C-O elongation) and 772 (folding of -CH2) cm^{-1} were identified [34–36].

Figure 3 schematizes the crosslinking reaction of DGEBA / MTHPA catalyzer system. From the correlation reaction with FTIR spectra, the indicatives of curing are associated by the oxirane ring opening presenting reduction in the band associated with -CH (3056 cm^{-1}) [33, 36, 37]; conversion of carbonyl and ether groups from anhydride in ester by esterification reactions (1872/1777 $\longrightarrow$ 1729 cm^{-1}) [36–41]; opening of oxirane ring by reaction of tertiary amines producing -OH (915 $\longrightarrow$ 3500 cm^{-1}) [36]; and insertion of primary and secondary amines (3500 and 3400 cm^{-1}) [38, 41].

For a quantitative analysis of the degree of conversion, a modification of Beer-Lambert law, Equation 14, was applied, taking into account the reference band area $A_{r\ 0\rightarrow t}$ and that associated with the functional groups converted during the cross-linking reaction $A_{c\ 0\rightarrow t}$ [36–38, 41].

$$\alpha = 1 - \frac{\left(\frac{A_C}{A_R}\right)_t}{\left(\frac{A_C}{A_R}\right)_0} \qquad (14)$$

Table 4 shows α values measured by the ratio between 915 cm^{-1}, 1729 cm^{-1} and 3056 cm^{-1} bands and the reference band 1510 cm^{-1} associated with -CH bonds of aromatic ring. Through oxirane ring opening at C-O bond identified by the decrease of 915 cm^{-1} band, and formation of ester groups

associated with the increase of 1729 cm^{-1} band, all compositions showed nearly complete conversion with α values higher than 98.33% and 92.77%, respectively. Concerning the decrease of 3056 cm^{-1} band related to CH elongation of oxirane ring, compositions E_{10} and EM_{10} presented conversion degree of 59.7% and 31.3% respectively, suggesting cross-linking was not effective for these systems. On the other hand, among the compositions with natural catalyzers, M_{10} presented α = 86.5%. Therefore this filler is the best option as a catalyzer for epoxy systems investigated in this work.

3.3. Cure kinetics

In order to select the better compositions for kinetics studies, non-isothermal DSC scans through several heating rates, acquired scans as presented in Figure 4 were used to evaluate the kinetics trends whereas the above models were applied to determine the kinetic parameters. In a previous study, the thermal degradation of epoxy resin started at approximately 285 °C [18].Around this temperature, the compositions E_{10} and EM_{10} degrade as the curing process takes place, hindering the cure kinetic evaluation. Thus, based on FTIR and non-isothermal DSC curve results, M_X and S_X compounds were selected to perform the kinetic study, due to their better cross-linking characteristics.

3.3.1. Ozawa model

Figure 5 shows the linear regression of ln β versus 1000/T_p of Ozawa model for S_X and M_X, from them the pre-exponential factor and E_a were evaluated and they are shown in Table 5. Synthetic compounds presented smaller deviation when compared to those upon membrane addition; this trend is most due linked to M_X non-linearity of T_p as a function of the heating rate as seen by Souza et al. [18]. This deviation suggests Ozawa model is inefficient to describe the cure reactions of biobased compounds investigated in this work.

A comparison between experimental and theoretical conversion degree computed using the Ozawa model are presented in Figure 6; for all analyzed composition failed fits were verified as also quantitatively shown in Figure S2. For S_2 composition a maximum deviation of approximately 25% between degrees of conversion in the range of 0.05-0.25 was observed, for M_{10} an acceptable adjustment applying 1 °C/min and 10 °C/min was reached, nevertheless, it is inadequate for the other rates. Ozawa model estimates a global activation energy computed by linear regression as a function of peak temperature, thus, for systems which have a significant deviation along the conversion, it is believed E_a changes along with the cure reactions what would explain the errors associated with S_X and M_X compounds [22, 23, 26].

3.3.2. Kissinger model

Another model applied in this work was developed by Kissinger, which determines E_a and the pre-exponential factor of cure reactions from the angular and linear coefficients of log (β/T_p^2) versus 1000/T_p, such regressions are shown in Figure 7. For all systems studied regressions resulted in similar behavior to that seen for the Ozawa model, mostly due to the dependence of both compositions on the heating and reaction rates [22, 27]. Lower deviations were observed for S_X compounds, suggesting the Kissinger model is invalid to describe the cure of M_X ones.

To (in)validate the Kissinger model, plots from raw DSC scans and those acquired using this model are shown in Figure 8. For both compositions, poor fits were observed, being more evidenced for M_{10} compound, which was expected due to the verified deviation in linear regressions. The discrepancy between theoretical and experimental data is presented in Figure S3, approximately, errors of 18% and 43% were verified for S_1 and M_5 respectively, proving the isoconversional models by integration methods, such as Ozawa and Kissinger, are unsuitable to describe S_X and M_X cure reactions, since they are limited to define systems that have constant E_a during the whole cure [6, 23].

3.3.3. Friedman isoconversional model

Figure 9 shows linear regression plots of ln ($d\alpha/dt$) versus $1000/T_p$ at several degrees of conversion, i.e., α = 0.11, 0.21, 0.31 … 0.91. From these plots, E_a and the pre-exponential factor were evaluated taking into a count the angular and linear coefficients of their equations, and these results are displayed in Figure 10. From E_a versus α and ln A versus α plots is verified both presented a similar profile since ln A can be determined as a function of E_a and the conversion rate. Table 5 presents the polynomial functions of these parameters.

E_a was analyzed taking conversion ranging from 0.1 to 0.9. For the synthetic compositions two steps were verified; the first one is occurring from 0.1 to 0.6, which is characterized by a substantially constant E_a indicating fast and easy cure process due to the reactive functional groups availability and the high and easily molecular mobility. In the second step (α = 0.6-0.9), E_a increased mostly due to competitive reactions, which led to a higher polymer viscosity increase, besides the reduction of reactive groups. This profile is an indication for autocatalytic reactions, in which this transition characterizes the change in the reaction which governs the system, being firstly controlled by the cure kinetics and in the final stages by diffusion [30].

From E_a plots were observed M_5 and M_{10} presented distinct trends. Despite the membrane action as catalyzer of DGEBA, for M_5 there was low availability of reactive groups to promote spontaneous reaction, so initially its cure required higher E_a to take place; as the polymerization proceeded reactive sites generated by esterification reactions provided synergism with membrane action decreasing E_a along with conversion range. In contrast, M_{10} followed similar behavior to that seen by Saeb, et al. [13] in DGEBA / MTHPA / EPIKURE / Eggshell compounds, in which Ea increased over the whole degree of conversion. According to the authors, as the reaction proceeds, there is a physical state changing, initially from liquid to rubbery (defined as gelation), then from rubbery to solid (defined as vitrification), decreasing the free volume and molecular mobility, and thus heading to higher E_a.

Through E_a (α) and ln A (α) functions, theoretical parameters from the Friedman model were measured. Figure 11 displays theoretical and experimental data for investigated compounds. For S_X, a quite good fit was reached at all applied heating rates along with the entire cure. Meanwhile, for M_X good fits were verified for M_5 at 2, 5, and 10 °C/min, most due to distinct kinetics of cross-linking reactions. Figure S4 illustrates quantitatively the discrepancy between experimental and theoretical data, errors lower than 1%, and 8% were observed for M_5 and S_5 compositions, respectively.

3.3.4. Friedman autocatalytic model

The reaction mechanism which best describes epoxy cure is got plotting ln [Af (α)] versus ln (1-α), such plots are shown in Figure 12 for S_2 and M_{10} at indicated heating rates; for linear regressions of S_2 a similar profile is observed for the heating rates 1-20 °C/min, showing linearity up to the inflection point in approximately -0.61 characterizing an autocatalytic reaction; when applying 1 °C/min is verified a linearity deviation ranging from -1.6 to -4.8 which may be associated with diffusion processes stronger evidenced during final stages of cure and for low heating rates [30]. On the other hand, for M_{10}, despite its similar profiles with the maximum points ranging from -0.35 to -0.13, presented deviation in ln [Af (α)] of -1.03, 6.63 and 0.99 for 1, 10 and 20 °C/min, respectively; suggesting for membrane's compounds the cure kinetic changes with the heating rates.

Plots of theoretical and experimental data for S_2 and M_5 compounds, as well as the associated error using Friedman autocatalytic model, are shown in Figure 13 and Figure S5. As above verified using Friedman isoconversional model, for S_X theoretical and experimental plots fit quite well, which is corroborated with a discrepancy lower than 5% for S_2. For M_5 theoretical data fitted at 2, 5, and 10 °C/min with an error close to 10%, which makes this an acceptable model to describe the curing process of these compounds.

3.3.5. Málek model

Figure 14 shows plots of Y (α) and Z (α) functions over the entire investigated conversion range. To determine the cure mechanism, the maximum points α_m and α_p were defined as well as the plot profile; in both systems, S_X and M_X, plots presented concave profile following the criterion $0 < \alpha_m < \alpha_p \neq 0.632$, indicating the cure for these compounds has autocatalytic character [42–44].

To evaluate the kinetic parameters and theoretical plots, E_a computed from Friedman Isoconversional model and p data acquired from the maximum point of y (α), α_m were applied. Comparison between theoretical and experimental plots as well as their discrepancy are shown in Figure 15 and Figure S6. For this model, both systems presented a reasonable fit in all applied heating rates. For S_5, a discrepancy lower than 8% at 1 and 2 °C/min were verified whereas for M_5 except at 1 °C/min data lower than 10% were obtained.

Some researchers previously applied evaluation of cure kinetics in DGEBA resins using Málek model, Zheng et al. [43] carried out the cure kinetics analysis of DGEBA/4,4'-methylenedianiline/multiwalled carbon nanotubes (MWCNT) system, it was observed for all composites and investigated rates corresponding results to $0 < \alpha_m < \alpha_p \neq 0.632$, indicating an autocatalytic reaction, in that work the theoretical and experimental plots fitted quite well. In another work conducted by Zabihi et al., the cure kinetics of DGEBA/polypropylenimine octaamine dendrimer/iron oxide II system, from Y (α) and Z (α) functions the maximum points of α_m and α_p plots were obtained, presenting 0.31 and 0.51 values, characterizing an autocatalytic reaction, theoretical and experimental plots also fitted very well validating the model for the investigated systems.

3.3.6. Models comparison

Table 6 shows the kinetic parameters measured using several models for S_X and M_X compounds. For all analyzed compounds, parameter n + m presented values higher than 1, indicating these are reactions with a complex character, however from these models, it was not possible to define the parameters trend [13, 21]. Membrane compositions showed E_a higher than S_X, decreasing its value upon increasing the filler content, suggesting the biobased rather filler amount can be a cure improver. Related to S_X compounds E_a decreased in S_2 whereas increased in S_5, nevertheless an increase of 1.68 in the frequency factor was observed when comparing S_2 and S_5, suggesting, despite S_5 requiring higher E_a to carry out the cure reaction, possibly there are higher collisions rate between reactive molecules accelerating the cure.

In order to select the most appropriate model for the description of developed compounds, a comparison between the experimental and theoretical data was made, as well as the discrepancies for S_5 and M_{10}, as shown in Figure 16 and Figure 17, respectively. The fit for isoconversional models by integration methods, Ozawa and Kissinger did not present a good fit with a maximum error of 15%. As earlier discussed, this is a limitation of these models since they consider E_a constant. Nevertheless, it was observed in Figure 10 that this parameter varies along with the conversion rate, justified the inadequacy of both equations. Málek, Friedman model-based, and Friedman isoconversional models presented a good fit, with a discrepancy lower than 5%.

Zhou et al. [26] verified the nonconformity of integration isoconversional models, et al. [26] in a comparative work using Ozawa and Friedman Models to describe the cure kinetics of DGEBA/2-ethyl-4-methylimidazole/carborundum compound; due to the determination of constant E_a Ozawa model was not representative for describing the experimental results, while the second model gave an E_a decreasing during the cure. Contrarily, Friedman presented a good fit with small deviations at the end of the cure being more evident in lower rates, due to the change in the reaction control where diffusion processes are more evidenced under these conditions.

Because of E_a dependence with the degree of conversion for M_X and S_X compounds, Ozawa and Kissinger models did not present a good fit with errors higher than 30%, as shown in Figure 17. For Friedman isoconversional model, it failed for some rates, which indicates the cure of M_X compounds

depends on E_a as also the availability of reactive functional groups throughout the cross-linking process, being the last one controlled by f (α). Thus, Málek and Friedman based models presented a smaller error, about 10%, between theoretical and experimental data.

Saeb et al. [13] performed a kinetic study applying several models for DGEBA/MTHPA/EPIKURE/eggshell system in that work authors observed a poor fit for Friedman isoconversional model, because in the final stages the reaction is diffusion controlled implying in a changeable E_a. Málek model also did not present good results, unlike what was evaluated for M_X compounds, it was assumed E_a constant evaluated by the Ozawa model promoting such error. Nevertheless, Friedman model-based was able to provide a good fit between experimental and theoretical results.

4. Conclusions

Compositions with synthetic catalyzer DEH 35 (S_X) and with natural eggshell (E_X), eggshell/membrane (EM_X), and membrane (M_X) bio-fillers were successfully produced and extremelly good dispersion was reached as seen in SEM images. Both the eggshell and membrane have essential elements for curing. However, as evident in the FTIR results, only the membrane presented a potential application in cross-linking performance.

Related to kinetic models, Ozawa and Kissinger were not able to describe the cross-linking process of S_X and M_X compounds, since these systems have changeable E_a. Friedman isoconversional showed more significant deviations for M_X compounds due to the change in the cure kinetic control, which in the final stages are diffusion controlled, as also due to linearity deviation of cross-linking temperature as a function of the heating rate. Therefore, the Friedman Model-Based and Málek models were the most suitable for describing the S_X and M_X compounds.

Funding

The authors would like to acknowledge the financial support from the Coordenação de Aperfeiçoamento de Pessoal de Nível Superior (CAPES) and from CNPq (Conselho Nacional de Desenvolvimento Científico e Tecnológico)

Acknowledgement

The authors would like to thank Olin Corporation (Brazil) for kindly supplying the reactants.

References

[1] S. Kumar, S. Krishnan, S. K. Samal, S. Mohanty, S. K. Nayak, Toughening of petroleum based (dgeba) epoxy resins with various renewable resources based flexible chains for high performance applications: A review, Industrial & Engineering Chemistry Research 57 (8) (2018) 2711–2726.

[2] J. Pascault, R. Williams, Epoxy Polymers: New Materials and Innovations, Wiley, 2009.

[3] C. Uglea, Oligomer Technology and Applications, Plastics Engineering, Taylor & Francis, 1998.

[4] J. Kim, J. Kim, S. Song, S. Zhang, J. Cha, K. Kim, H. Yoon, Y. Jung, K.-W. Paik, S. Jeon, Strength dependence of epoxy composites on the average filler size of non-oxidized graphene flake, Carbon 113 (2017) 379–386.

[5] G. R. Saad, A. A. Ezz, H. A. Ahmed, Cure kinetics, thermal stability, and dielectric properties of epoxy/barium ferrite/polyaniline composites, Thermochimica acta 599 (2015) 84–94.

[6] L. Li, Z. Zeng, H. Zou, M. Liang, Curing characteristics of an epoxy resin in the presence of functional graphite oxide with amine-rich surface, Thermochimica acta 614 (2015) 76–84.

[7] L. Rajabi, M. Marzban, A. A. Derakhshan, Epoxy/alumoxane and epoxy/boehmite nanocomposites: cure behavior, thermal stability, hardness and fracture surface morphology, Iranian Polymer Journal 23 (3) (2014) 203–215.

[8] S. Ghorabi, L. Rajabi, S. S. Madaeni, S. Zinadini, A. A. Derakhshan, Effects of three surfactant types of anionic, cationic and non-ionic on tensile properties and fracture surface morphology of epoxy/mwcnt nanocomposites, Iranian Polymer Journal 21 (2) (2012) 121–130.

[9] M. Panchal, G. Raghavendra, M. O. Prakash, S. Ojha, P. S. C. Bose, Moisture absorption behavior of treated and untreated eggshell particulate epoxy composites, Silicon (2018) 1–9.

[10] C. M. Vu, H. J. Choi, Fracture toughness and surface morphology of micro/nano sized fibrils-modified epoxy resin, Polymer Science Series A 58 (3) (2016) 464–470.

[11] H. Deka, T. Wang, A. K. Mohanty, M. Misra, Novel biocomposites from biobased epoxy and corn-based distillers dried grains (ddg), Journal of Polymers and the Environment 23 (4) (2015) 425–436.

[12] M. R. Saeb, H. Rastin, M. Nonahal, S. M. R. Paran, H. A. Khonakdar, D. Puglia, Cure kinetics of epoxy/chicken eggshell biowaste composites: Isothermal calorimetric and chemorheological analyses, Progress in Organic Coatings 114 (2018) 208–215.

[13] M. R. Saeb, M. Ghaffari, H. Rastin, H. A. Khonakdar, F. Simon, F. Najafi, V. Goodarzi, D. Puglia, F. H. Asl, K. Formela, et al., Biowaste chicken eggshell powder as a potential cure modifier for epoxy/anhydride systems: competitiveness with terpolymer-modified calcium carbonate at low loading levels, RSC Advances 7 (4) (2017) 2218–2230.

[14] Pesquisa trimestral de produção de ovos de galinha (2018).
URL https://www.ibge.gov.br/estatisticas-novoportal/economicas/agricultura-e-pecuaria/9216-pesquisa-trimestral -da-producao-de-ovos-de-galinha.html?edicao=20753t=downloads

[15] Y. Mine, Egg Bioscience and Biotechnology, Wiley, 2008.
URL https://books.google.com.br/books?id=OnZNqXI8zpoC

[16] M.-T. Ton-That, T.-D. Ngo, P. Ding, G. Fang, K. Cole, S. Hoa, Epoxy nanocomposites: Analysis and kinetics of cure, Polymer Engineering & Science 44 (6) (2004) 1132–1141.

[17] F. Mustata, N. Tudorachi, D. Rosu, Thermal behavior of some organic/inorganic composites based on epoxy resin and calcium carbonate obtained from conch shell of rapana thomasiana, Composites Part B: Engineering 43 (2) (2012) 702–710.

[18] J. W. d. L. Souza, N. G. Jaques, M. Popp, J. Kolbe, M. V. L. Fook, R. M. R. Wellen, Optimization of epoxy resin: An investigation of eggshell as a synergic filler, Materials 12 (9) (2019) 1489.

[19] H. L. Friedman, Kinetics of thermal degradation of char-forming plastics from thermogravimetry. application to a phenolic plastic, in: Journal of Polymer Science Part C: Polymer Symposia, Vol. 6, Wiley Online Library, 1964, pp. 183–195.

[20] M. Ghaffari, M. Ehsani, H. A. Khonakdar, G. Van Assche, H. Terryn, Evaluation of curing kinetic parameters of an epoxy/polyaminoamide/nano-glassflake system by non-isothermal differential scanning calorimetry, Thermochimica acta 533 (2012) 10–15.

[21] S. H. Ryu, J. Sin, A. Shanmugharaj, Study on the effect of hexamethylene diamine functionalized graphene oxide on the curing kinetics of epoxy nanocomposites, European Polymer Journal 52 (2014) 88–97.

[22] J. M. Criado Luque, P. E. Sánchez Jiménez, L. A. Pérez Maqueda, Critical study of the isoconversional methods of kinetic analysis, Journal of thermal Analysis and Calorimetry, 92, 1-17. (2008).

[23] P. Šimon, Isoconversional methods, Journal of Thermal Analysis and Calorimetry 76 (1) (2004) 123.

[24] T. Ozawa, A new method of analyzing thermogravimetric data, Bulletin of the chemical society of Japan 38 (11) (1965) 1881–1886.

[25] H. E. Kissinger, Reaction kinetics in differential thermal analysis, Analytical chemistry 29 (11) (1957) 1702–1706.

[26] T. Zhou, M. Gu, Y. Jin, J. Wang, Studying on the curing kinetics of a dgeba/emi-2, 4/nano-sized carborundum system with two curing kinetic methods, Polymer 46 (16) (2005) 6174–6181.

[27] S. Montserrat, C. Flaque, M. Calafell, G. Andreu, J. Malek, Influence of the accelerator concentration on the curing reaction of an epoxy-anhydride system, Thermochimica Acta 269 (1995) 213–229.

[28] S. Montserrat, F. Román, J. Hutchinson, L. Campos, Analysis of the cure of epoxy based layered silicate nanocomposites: reaction kinetics and nanostructure development, Journal of applied polymer science 108 (2) (2008) 923–938.

[29] G. Senum, R. Yang, Rational approximations of the integral of the arrhenius function, Journal of thermal analysis and calorimetry 11 (3) (1977) 445–447.

[30] M. Nonahal, H. Rastin, M. R. Saeb, M. G. Sari, M. H. Moghadam, P. Zarrintaj, B. Ramezanzadeh, Epoxy/pamam dendrimer-modified graphene oxide nanocomposite coatings: Nonisothermal cure kinetics study, Progress in Organic Coatings 114 (2018) 233–243.

[31] A. Shanmugharaj, S. H. Ryu, Study on the effect of aminosilane functionalized nanoclay on the curing kinetics of epoxy nanocomposites, Thermochimica acta 546 (2012) 16–23.

[32] T. Zhou, M. Gu, Y. Jin, J. Wang, Effects of nano-sized carborundum particles and amino silane coupling agent on the cure reaction kinetics of dgeba/emi-2, 4 system, Polymer 46 (16) (2005) 6216–6225.

[33] M. G. González, J. C. Cabanelas, J. Baselga, Applications of ftir on epoxy resins-identification, monitoring the curing process, phase separation and water uptake, Infrared Spectroscopy-Materials Science, Engineering and Technology 2 (2012) 261–284.

[34] R. M. Silverstein, G. C. Bassler, Spectrometric identification of organic compounds, Journal of Chemical Education 39 (11) (1962) 546.

[35] N. Tudorachi, F. Mustata, Curing and thermal degradation of diglycidyl ether of bisphenol a epoxy resin crosslinked with natural hydroxy acids as environmentally friendly hardeners, Arabian Journal of Chemistry (2017).

[36] G. Nikolic, S. Zlatkovic, M. Cakic, S. Cakic, C. Lacnjevac, Z. Rajic, Fast fourier transform ir characterization of epoxy gy systems crosslinked with aliphatic and cycloaliphatic eh polyamine adducts, Sensors 10 (1) (2010) 684–696.

[37] S. T. Cholake, M. R. Mada, R. S. Raman, Y. Bai, X. Zhao, S. Rizkalla, S. Bandyopadhyay, Quantitative analysis of curing mechanisms of epoxy resin by mid-and near-fourier transform infra red spectroscopy, Defence Science Journal 64 (3) (2014) 314–321.

[38] B. Montero, A. Serra, C. Ramírez, X. Ramis, Epoxy/anhydride networks modified with polyhedral oligomeric silsesquioxanes, Polymer composites 34 (1) (2013) 96–108.

[39] A. Rigail-Cedeño, C. S. P. Sung, Fluorescence and ir characterization of epoxy cured with aliphatic amines, Polymer 46 (22) (2005) 9378–9384.

[40] F. Fraga, S. Burgo, E. R. Núñez, Curing kinetic of the epoxy system badge n= 0/1, 2 dch by fourier transform infrared spectroscopy (ftir), Journal of Applied Polymer Science 82 (13) (2001) 3366–3372.

[41] M. C. Finzel, J. Delong, M. C. Hawley, Effect of stoichiometry and diffusion on an epoxy/amine reaction mechanism, Journal of Polymer Science Part A: Polymer Chemistry 33 (4) (1995) 673–689.

[42] X. Zheng, D. Li, C. Feng, X. Chen, Thermal properties and non-isothermal curing kinetics of carbon nanotubes/ionic liquid/epoxy resin systems, Thermochimica acta 618 (2015) 18–25.

[43] F. Román, Y. Calventus, P. Colomer, J. M. Hutchinson, Identification of nanostructural development in epoxy polymer layered silicate nanocomposites from the interpretation of differential scanning calorimetry and dielectric spectroscopy, Thermochimica acta 541 (2012) 76–85.

[44] O. Zabihi, A. Khodabandeh, S. Ghasemlou, Investigation of mechanical properties and cure behavior of dgeba/nano-fe2o3 with polyamine dendrimer, Polymer degradation and stability 97 (9) (2012) 1730–1736.

Figure 17: Comparative plots of experimental and theoretical data using indicated models for M_{10} at 2 °C/min, (a) conversion rate versus T and (b) Δ versus α

Table 1: Epoxy and Epoxy/eggshell compounds codification.

[1] Composition	Epoxy Resin	Hardener	Catalyzer			
	DER 331	MTHPA	DEH 35	Membrane	Eggshell	Eggshell+ Membrane
S_1	100	87	1	0	0	0
S_2	100	87	2	0	0	0
S_5	100	87	5	0	0	0
M_5	100	87	0	5	0	0
M_{10}	100	87	0	10	0	0
E_{10}	100	87	0	0	10	0
EM_{10}	100	87	0	0	0	10

[1] S: synthetic compounds. M: composites with membrane powder. E: composites with eggshell powder. EM: composites with eggshell and membrane powders.

Table 2: Cure temperature profiles of S_5, E_{10}, EM_{10}, and M_{10} compounds.

Time (h)	Temperature (°C)
2	80
4	120
2	140
4	160
2	170
4	190
2	200

Table 3: Identification of chemical elements by EDS in images presented in Figure 1.

Elements (%)	**Eggshell**	**Membrane**	**S_5**	**E_{10}**	**EM_{10}**	**M_{10}**
Carbon (C)	6.3	53.7	17.3	7.9	18.0	17.9
Sulfur (S)		12.6			1.3	0.3
Oxygen (O)	57.3	20.5	74.5	62.9	56.4	68.8
Calcium (Ca)	19.5			16.2	3.9	0.4
Nitrogen (N)	11.6	13.3	8.2	7.5	8.7	8.3
Chlorine (Cl)	1.1			0.8	1.8	
Sodium (Na)	2.1			1.4	2.8	
Silicon (Si)	1.1			2.9	6.6	

Phosphor (P)	1.0			0.3	0.2	

Table 4: Quantification of degree of conversion in several functional groups upon 1510 cm-1 reference.

	S_5 (%)	E_{10} (%)	EM_{10} (%)	M_{10} (%)
α (3056/1510)	91.0	59.7	31.3	86.5
α (915/1510)	99.8	99.1	98.3	99.8
α (1729/1510)	92.8	99.5	98.5	97.8

Table 5: E_a (α) and ln A (α) functions of S_X and M_X compounds.

Compounds	**Functions**
$\mathbf{S}_1$	$E_a\ \alpha = 77.081 - 27.416\alpha + 2.409*10^3\alpha^2 - 2.911*10^3\alpha^3 + 1.569*10^5\alpha^4 - 4.669*10^5\alpha^5 + 8.188*10^5\alpha^6 - 8.442*10^5\alpha^7 + 4.734*10^5\alpha^8 - 1.114*10^6\alpha^9$
	$lnA\ \alpha = 15.281 + 19.815\alpha + 451.518\alpha^2 - 7.037*10^3\alpha^3 + 4.048*10^4\alpha^4 - 1.239*10^5\alpha^5 + 2.209*10^5\alpha^6 - 2.301*10^5\alpha^7 + 1.301*10^5\alpha^8 - 3.082*10^4\alpha^9$
$\mathbf{S}_2$	$E_a\ \alpha = 62.782 + 271.076\alpha - 1.743*10^3\alpha^2 - 1.691*10^3\alpha^3 + 5.786*10^5\alpha^4 - 2.588*10^5\alpha^5 + 5.634*10^5\alpha^6 - 6.704*10^5\alpha^7 + 4.179*10^5\alpha^8 - 1.069*10^6\alpha^9$
	$lnA\ \alpha = 11.132 + 115.665\alpha - 887.005\alpha^2 + 1.923*10^3\alpha^3 + 7.396*10^3\alpha^4 - 5.216*10^4\alpha^5 + 1.283*10^3\alpha^6 - 1.617*10^5\alpha^7 + 1.042*10^5\alpha^8 - 2.725*10^4\alpha^9$
$\mathbf{S}_5$	$E_a\ \alpha = 73.387 + 143.346\alpha - 804.143\alpha^2 - 1.513*10^3\alpha^3 + 3.054*10^4\alpha^4 - 1.308*10^5\alpha^5 + 2.850*10^5\alpha^6 - 3.482*10^6\alpha^7 + 2.271*10^5\alpha^8 - 6.150*10^4\alpha^9$
	$lnA\ \alpha = 15.374 + 71.5416\alpha - 551.864\alpha^2 - 1.629*10^3\alpha^3 + 701.877\alpha^4 - 1.783*10^4\alpha^5 + 5.160*10^4\alpha^6 - 7.175*10^4\alpha^7 + 5.060*10^4\alpha^8 - 1.445*10^4\alpha^9$
$\mathbf{M}_5$	$E_a\ \alpha = 233.88 + 77.535\alpha - 1.082*10^4\alpha^2 + 9.814*10^4\alpha^3 - 4.474*10^5\alpha^4 + 1.171*10^6\alpha^5 - 1.834*10^6\alpha^6 + 1.701*10^6\alpha^7 - 8.626*10^5\alpha^8 + 1.843*10^4\alpha^9$
	$lnA\ \alpha = 52.039 + 2.470\alpha - 2.536*10^3\alpha^2 + 2.367*10^4\alpha^3 - 1.091*10^5\alpha^4 + 2.873*10^5\alpha^5 - 4.517*10^5\alpha^6 + 4.201*10^5\alpha^7 - 2.134*10^5\alpha^8 + 4.566*10^4\alpha^9$

$\mathbf{M}_{10}$	$E_a\ \alpha = 79.517 - 18.053\alpha + 3.541*10^3\alpha^2 - 4.022*10^4\alpha^3 + 2.146*10^5\alpha^4 - 6.352*10^5\alpha^5 + 1.104*10^6\alpha^6 - 1.119*10^6\alpha^7 + 6.116*10^5\alpha^8 - 1.386*10^4\alpha^9$
	$lnA\ \alpha = 12.857 + 20.673\alpha + 572.044\alpha^2 - 7.856*10^3\alpha^3 + 4.448*10^4\alpha^4 - 1.354*10^5\alpha^5 + 2.396*10^5\alpha^6 - 2.460*10^5\alpha^7 + 1.357*10^5\alpha^8 - 3.107*10^4\alpha^9$

Table 6: Kinetic parameters of S_X and M_X at indicated models.

Compounds		Friedman Model-Based	Málek	Ozawa	Kissinger	Friedman Isoconversional
S_1	E_a (kJ/mol)	76.16	78.92	77.30	77.44	78.92
	ln A	17.42	17.11	17.34	17.07	17.71
	n+m	1.57	2.11	-	-	-
	R^2	0.990	-	0.888	0.921	0.995
S_2	E_a (kJ/mol)	70.18	71.99	69.61	69.72	71.99
	ln A	16.30	16.15	15.36	15.07	16.02
	n+m	1.92	2.00	-	-	-
	R^2	0.996	-	0.863	0.893	0.997
S_5	E_a (kJ/mol)	74.01	85.89	76.52	75.95	85.89
	ln A	17.98	20.00	17.88	17.67	20.86
	n+m	1.66	2.57	-	-	-
	R^2	0.995	-	0.912	0.910	0.990
M_5	E_a (kJ/mol)	127.26	109.36	93.87	92.56	109.36
	ln A	24.92	22.47	17.08	16.52	20.38
	n+m	1.75	1.58	-	-	-
	R^2	0.975	-	0.933	0.932	0.999
M_{10}	E_a (kJ/mol)	93.13	119.77	79.40	79.77	119.77
	ln A	17.32	14.33	14.04	13.86	23.49
	n+m	2.50	1.69	-	-	-
	R^2	0.897	-	0.900	0.826	0.971

The authors declare that they have no conflict of interests or personal relationships that could have appeared to influence the work reported in this paper.

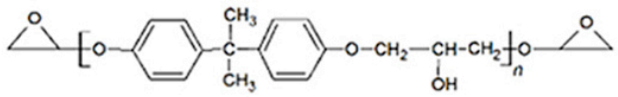

DGEBA

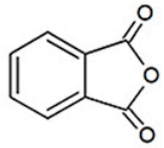

MTHPA

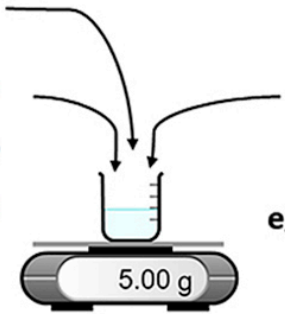

Eggshell and/or eggshell membrane

DSC Analysis

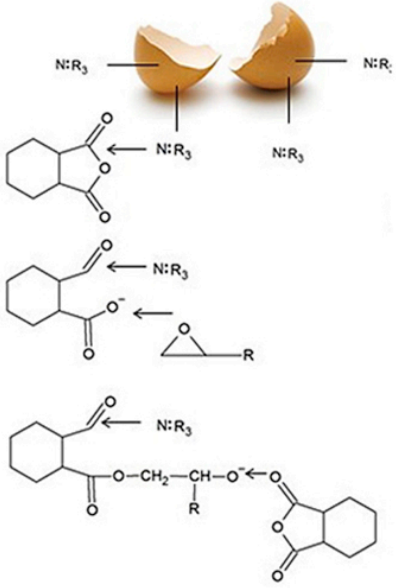

Epoxy/eggshell cure reaction

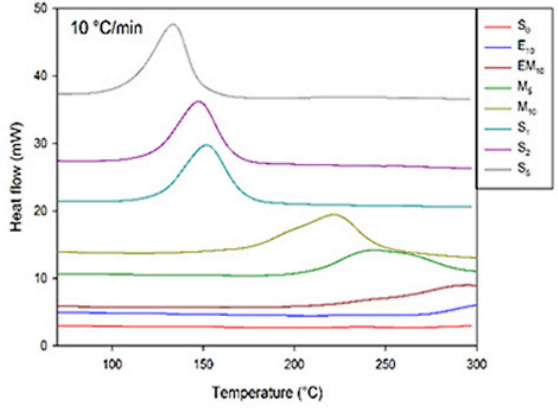

Cure kinetic models

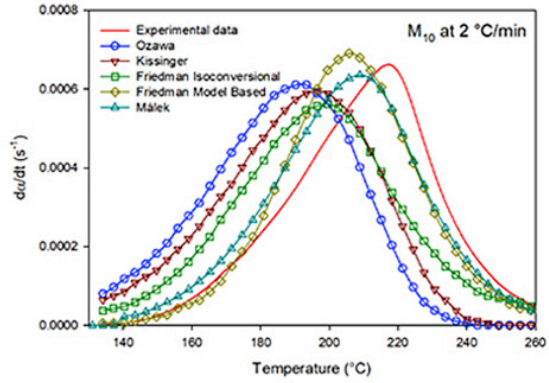

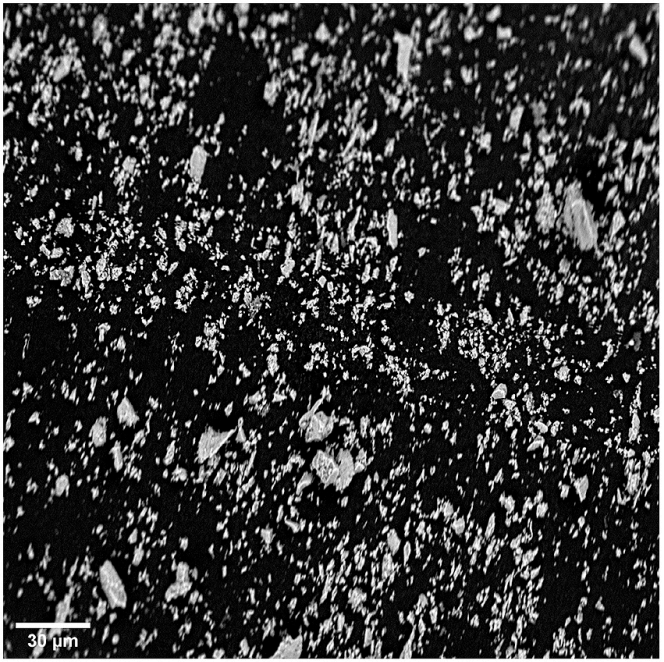

(a)

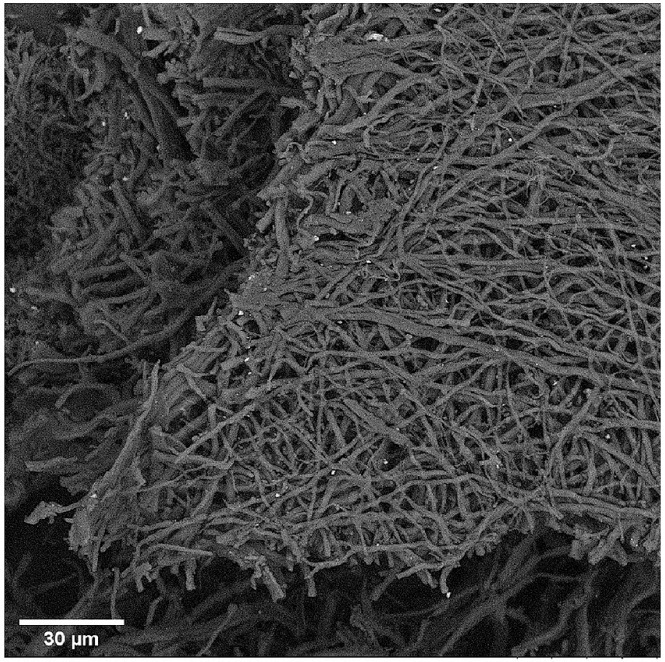

(b)

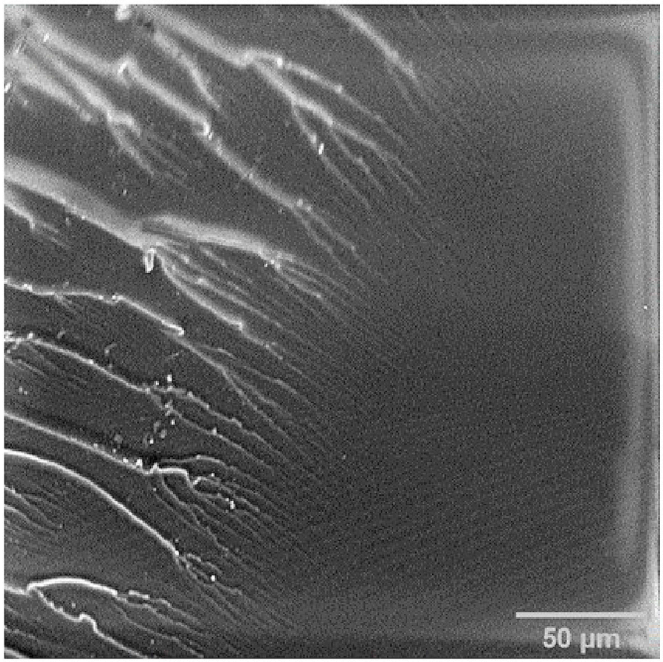

(c)

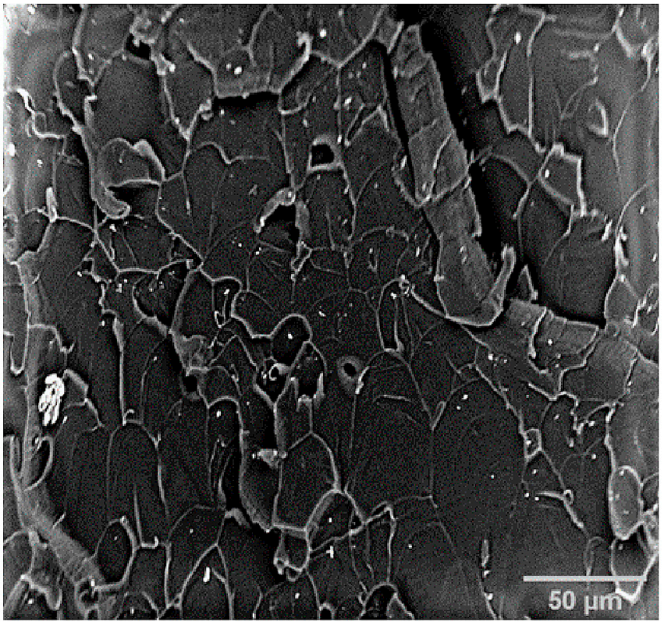

(d)

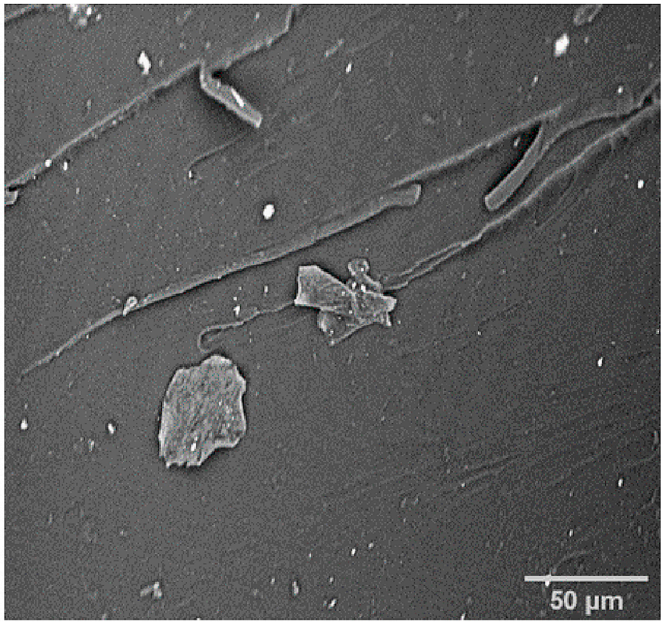

(e)

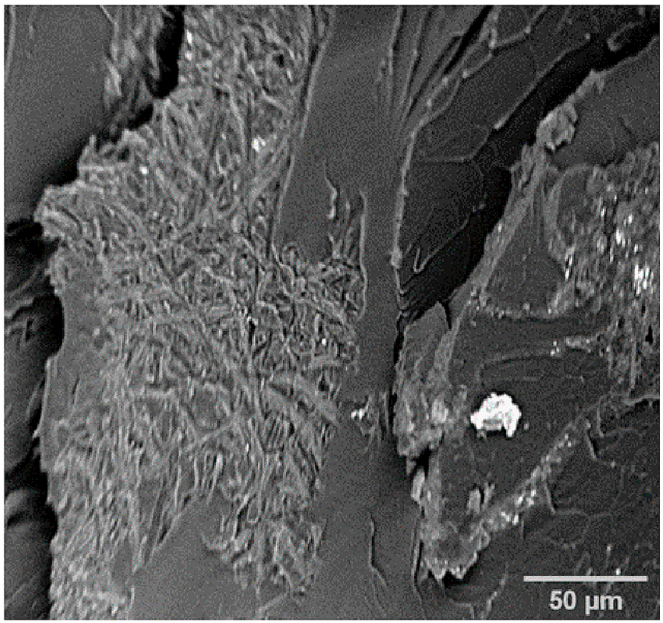

(f)

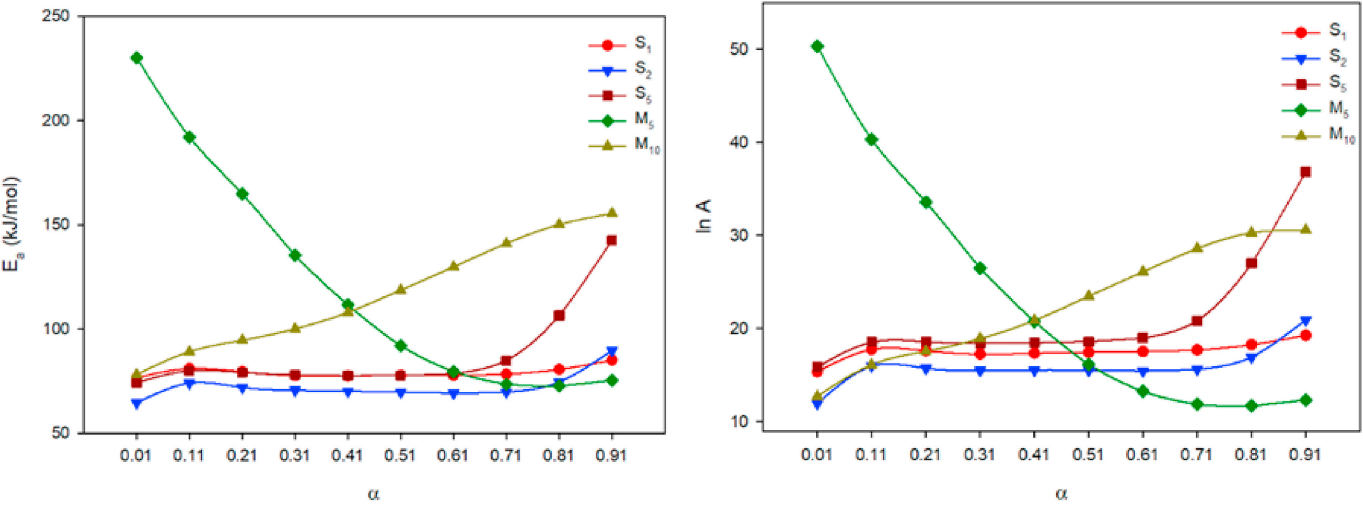
250
200
150
100
50
E_a (kJ/mol)
0.01
0.11
0.21
0.31
0.41
0.51
0.61
0.71
0.81
0.91
α
S_1
S_2
S_5
M_5
M_{10}
50
40
30
20
10
ln A
0.01
0.11
0.21
0.31
0.41
0.51
0.61
0.71
0.81
0.91
α
S_1
S_2
S_5
M_5
M_{10}

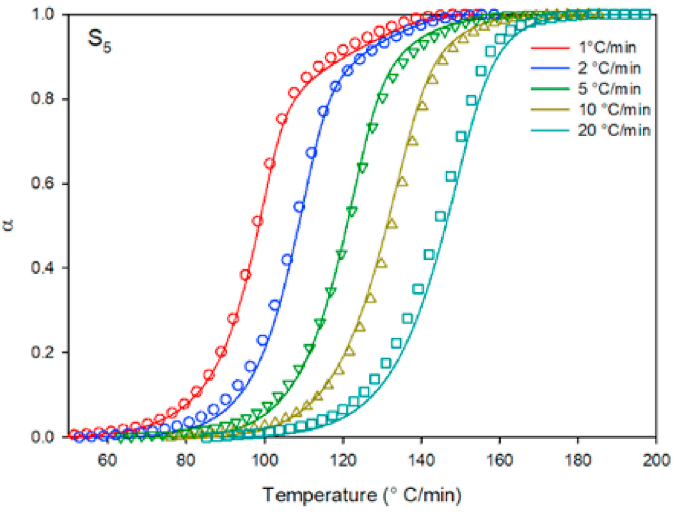
S5
1°C/min
2 °C/min
5 °C/min
10 °C/min
20 °C/min
α
Temperature (° C/min)

(a)

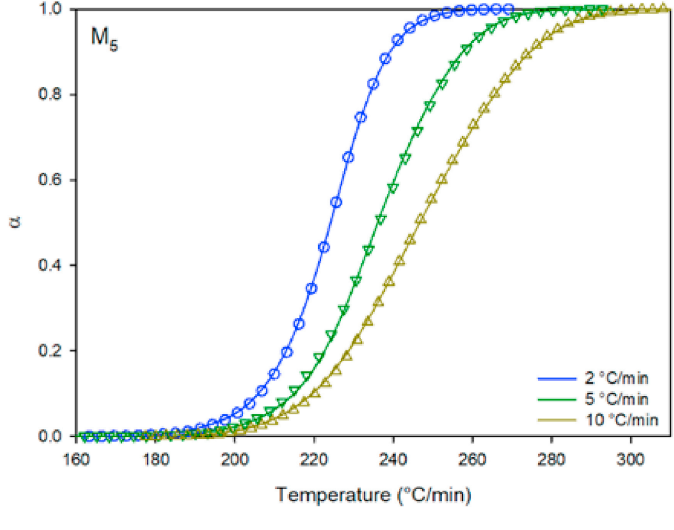
M5
2 °C/min
5 °C/min
10 °C/min
α
Temperature (°C/min)

(b)

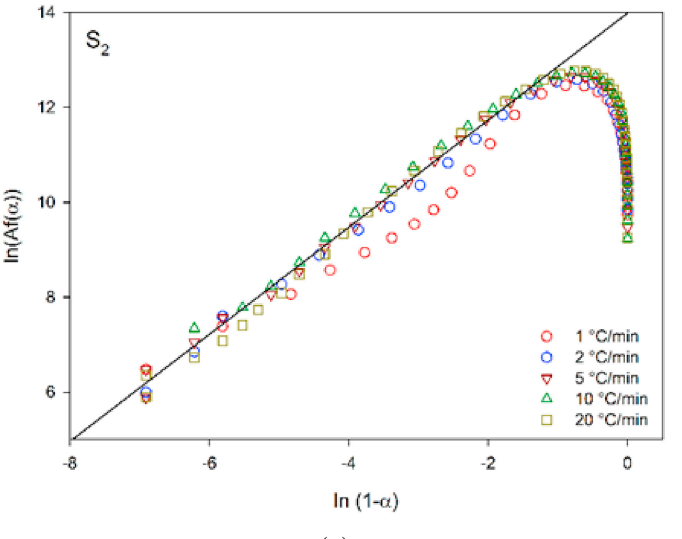
S2
ln(Af(α))
ln (1-α)
1 °C/min
2 °C/min
5 °C/min
10 °C/min
20 °C/min

(a)

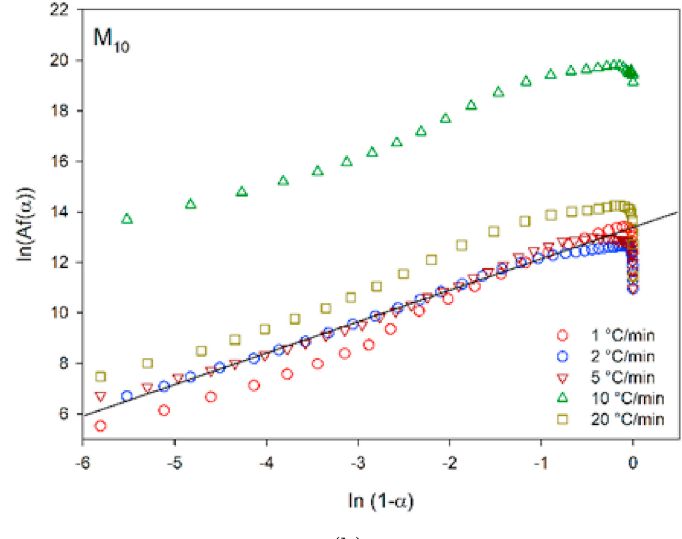
M10
ln(Af(α))
ln (1-α)
1 °C/min
2 °C/min
5 °C/min
10 °C/min
20 °C/min

(b)

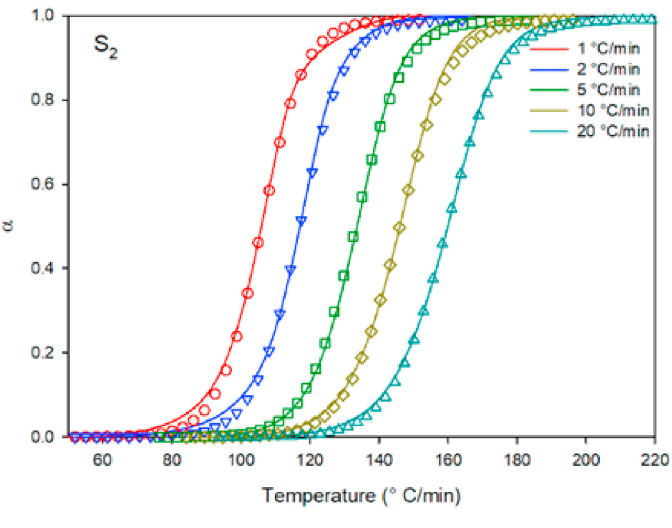
S2
1 °C/min
2 °C/min
5 °C/min
10 °C/min
20 °C/min
α
Temperature (° C/min)

(a)

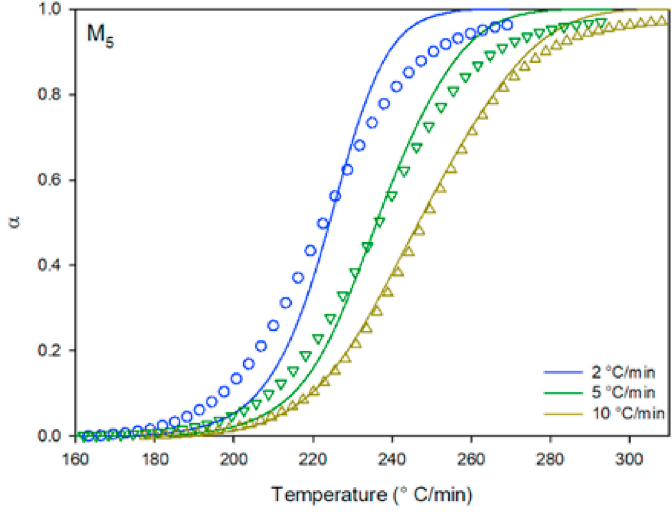
M5
2 °C/min
5 °C/min
10 °C/min
α
Temperature (° C/min)

(b)

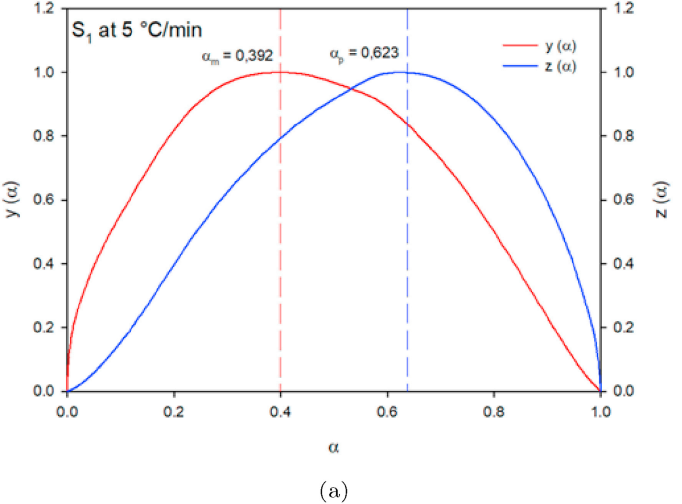
S1 at 5 °C/min
αm = 0,392
αp = 0,623
y (α)
z (α)
α

(a)

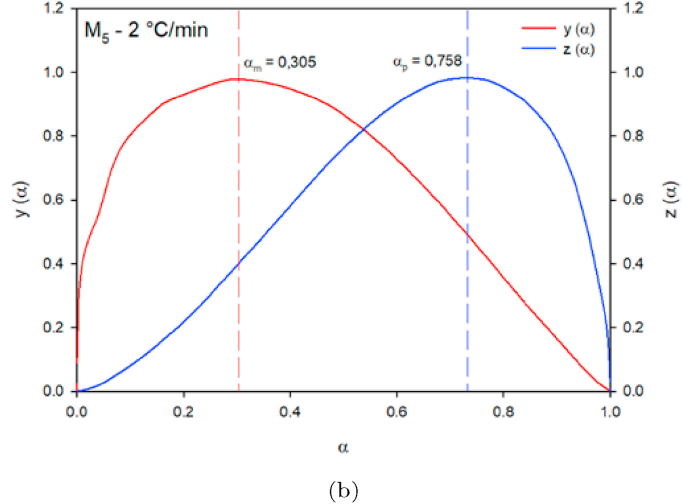
M5 - 2 °C/min
αm = 0,305
αp = 0,758
y (α)
z (α)
α

(b)

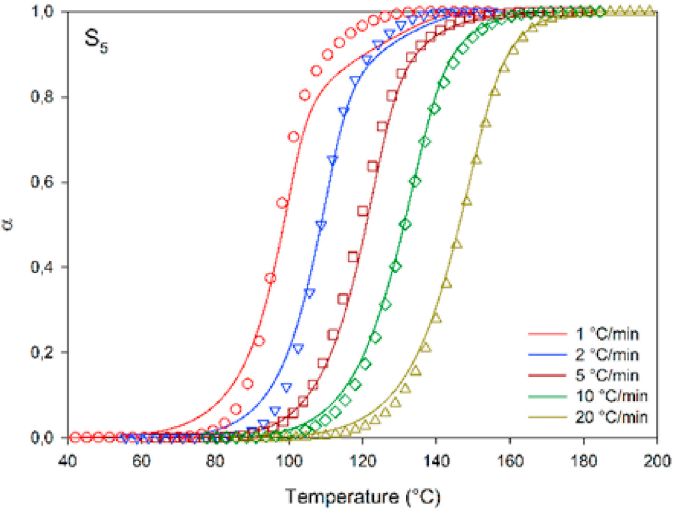
S5
α
1,0
0,8
0,6
0,4
0,2
0,0
40
60
80
100
120
140
160
180
200
Temperature (°C)
1 °C/min
2 °C/min
5 °C/min
10 °C/min
20 °C/min

(a)

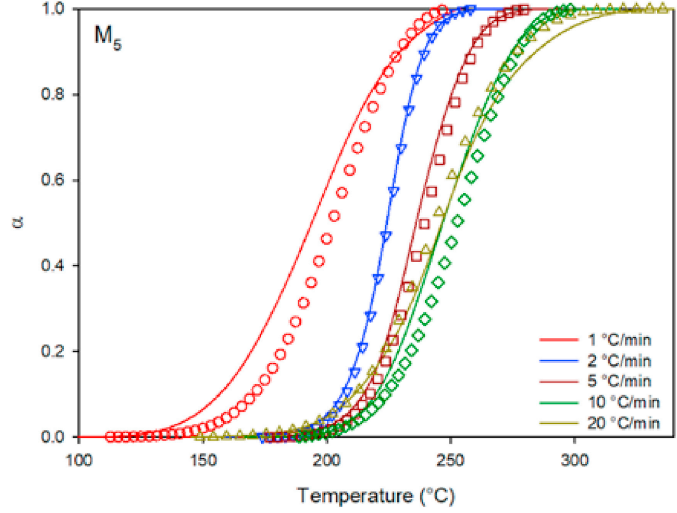
M5
α
1.0
0.8
0.6
0.4
0.2
0.0
100
150
200
250
300
Temperature (°C)
1 °C/min
2 °C/min
5 °C/min
10 °C/min
20 °C/min

(b)

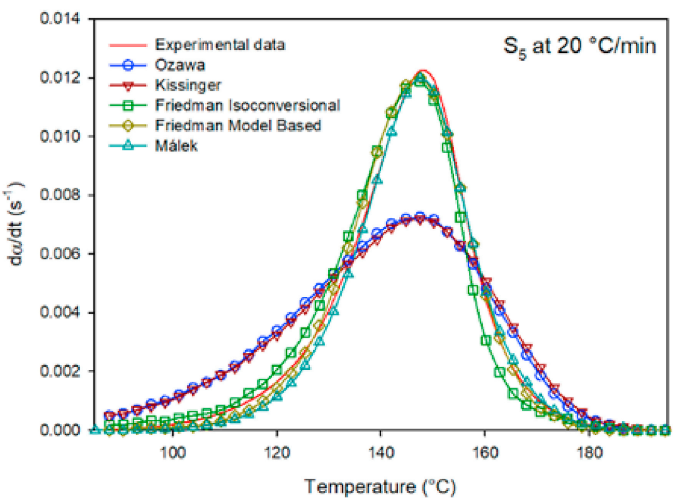
Experimental data
Ozawa
Kissinger
Friedman Isoconversional
Friedman Model Based
Málek
S5 at 20 °C/min
dα/dt (s-1)
0.014
0.012
0.010
0.008
0.006
0.004
0.002
0.000
100
120
140
160
180
Temperature (°C)

(a)

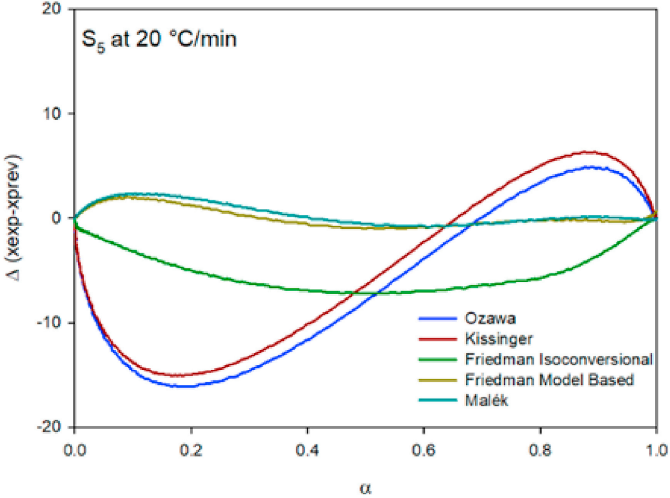
S5 at 20 °C/min
Δ (xexp-xprev)
20
10
0
-10
-20
0.0
0.2
0.4
0.6
0.8
1.0
α
Ozawa
Kissinger
Friedman Isoconversional
Friedman Model Based
Malék

(b)

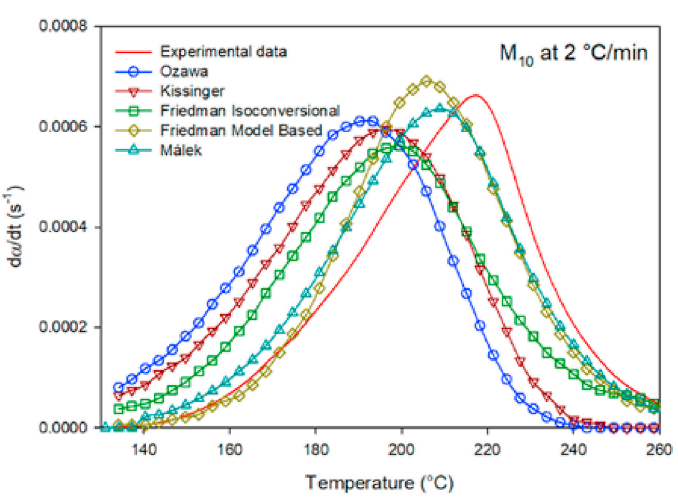
Experimental data
Ozawa
Kissinger
Friedman Isoconversional
Friedman Model Based
Málek
M10 at 2 °C/min
dα/dt (s-1)
Temperature (°C)
0.0008
0.0006
0.0004
0.0002
0.0000
140
160
180
200
220
240
260

(a)

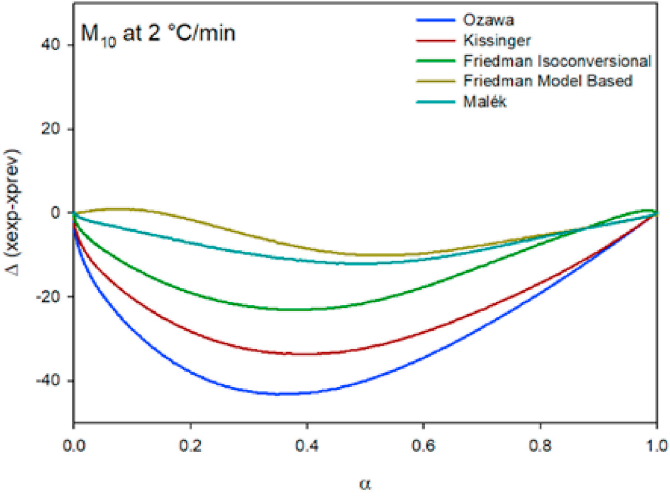
M10 at 2 °C/min
Ozawa
Kissinger
Friedman Isoconversional
Friedman Model Based
Malék
Δ (xexp-xprev)
α
40
20
0
-20
-40
0.0
0.2
0.4
0.6
0.8
1.0

(b)

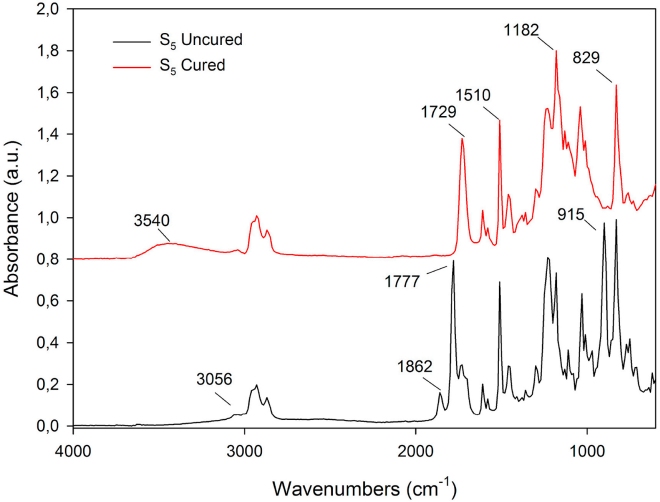
S5 Uncured
S5 Cured
1182
829
1510
1729
3540
915
1777
1862
3056
Absorbance (a.u.)
Wavenumbers (cm-1)

(a)

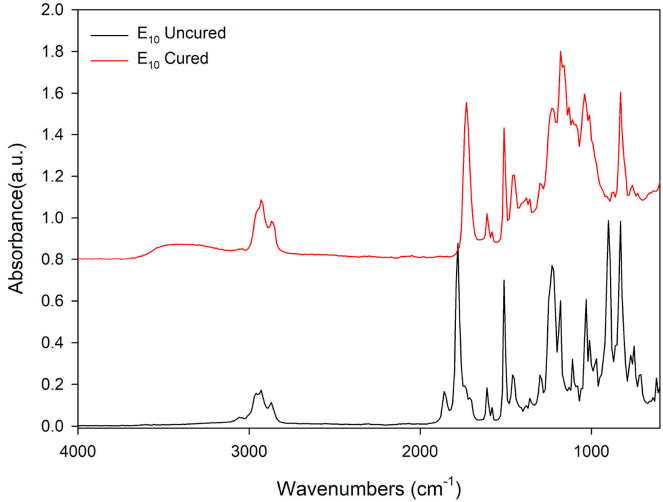
E10 Uncured
E10 Cured
Absorbance(a.u.)
Wavenumbers (cm-1)

(b)

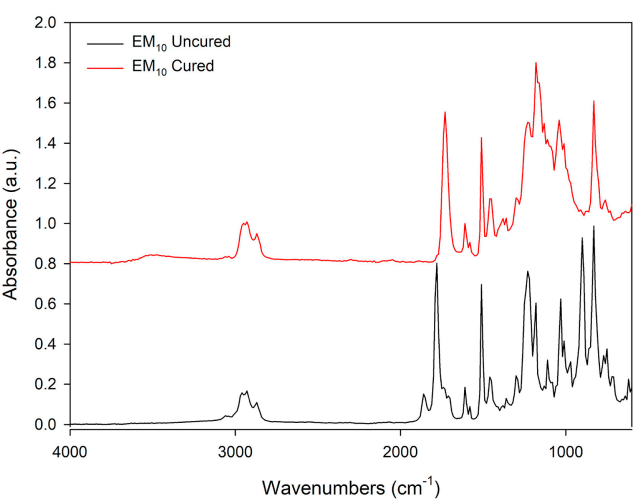
EM10 Uncured
EM10 Cured
Absorbance (a.u.)
Wavenumbers (cm-1)

(c)

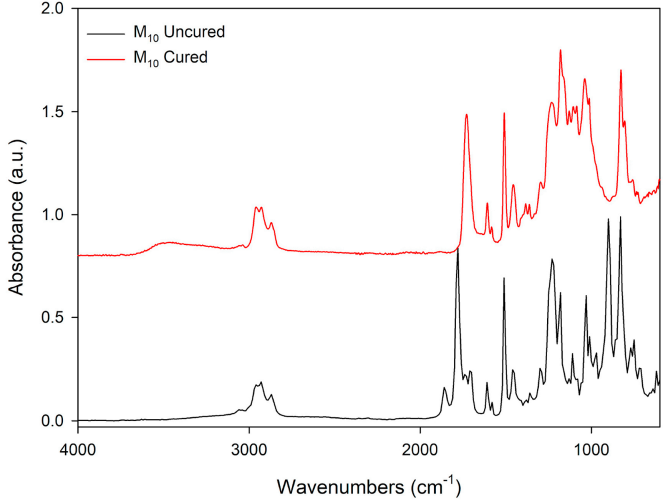
M10 Uncured
M10 Cured
Absorbance (a.u.)
Wavenumbers (cm-1)

(d)

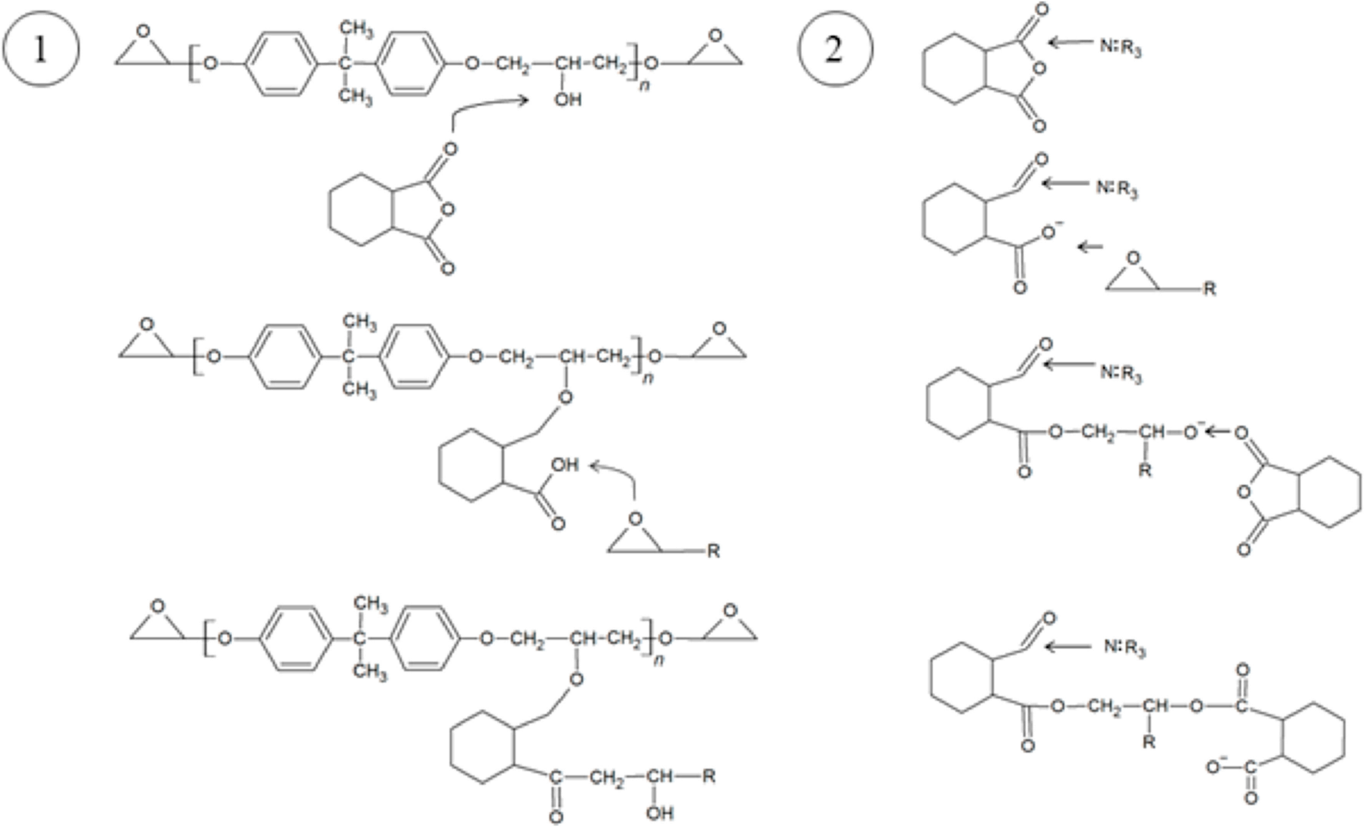
1
2
N:R3
R
OH
n

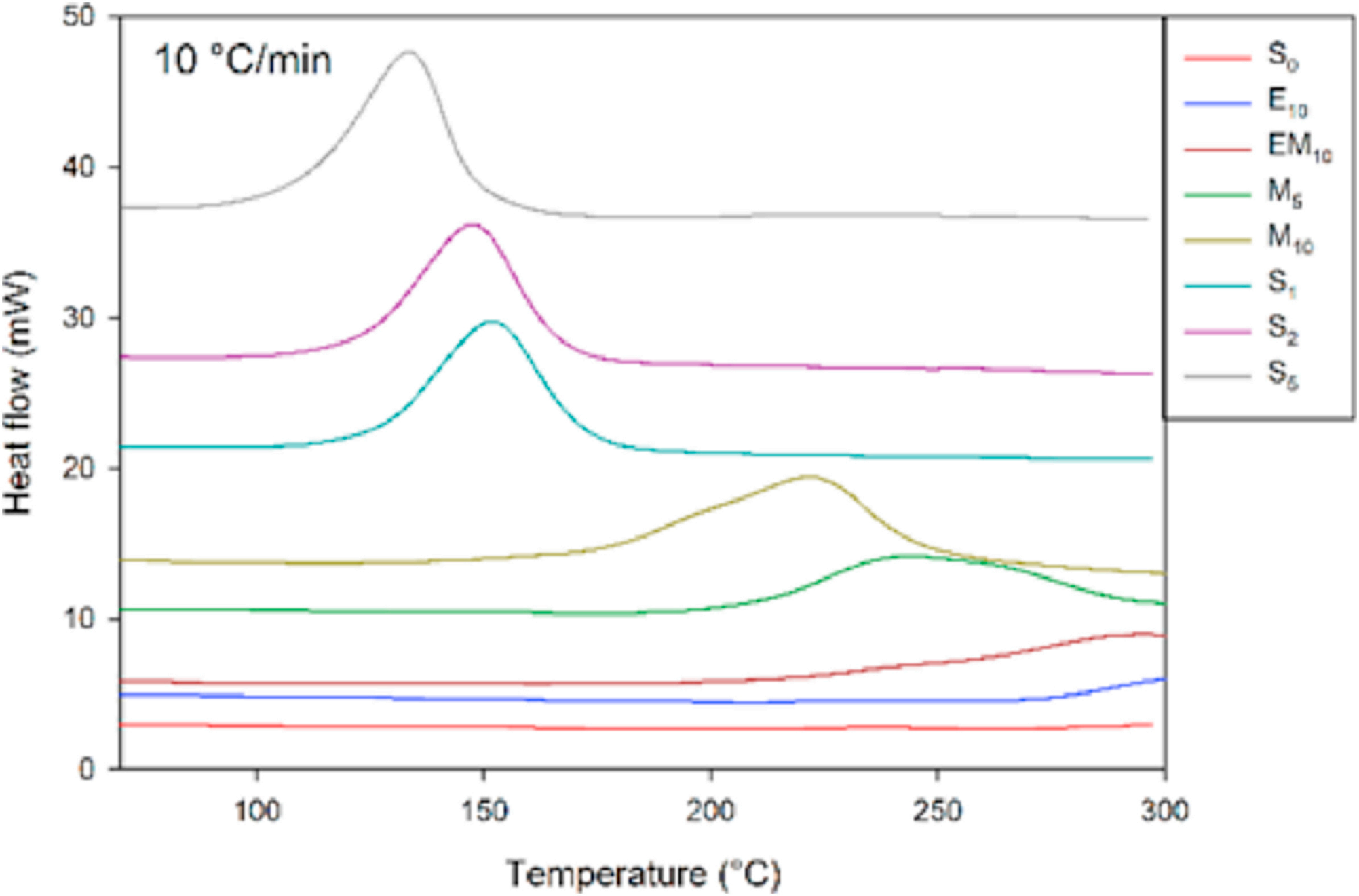
10 °C/min
Heat flow (mW)
Temperature (°C)
0
10
20
30
40
50
100
150
200
250
300
S_0
E_{10}
EM_{10}
M_5
M_{10}
S_1
S_2
S_5

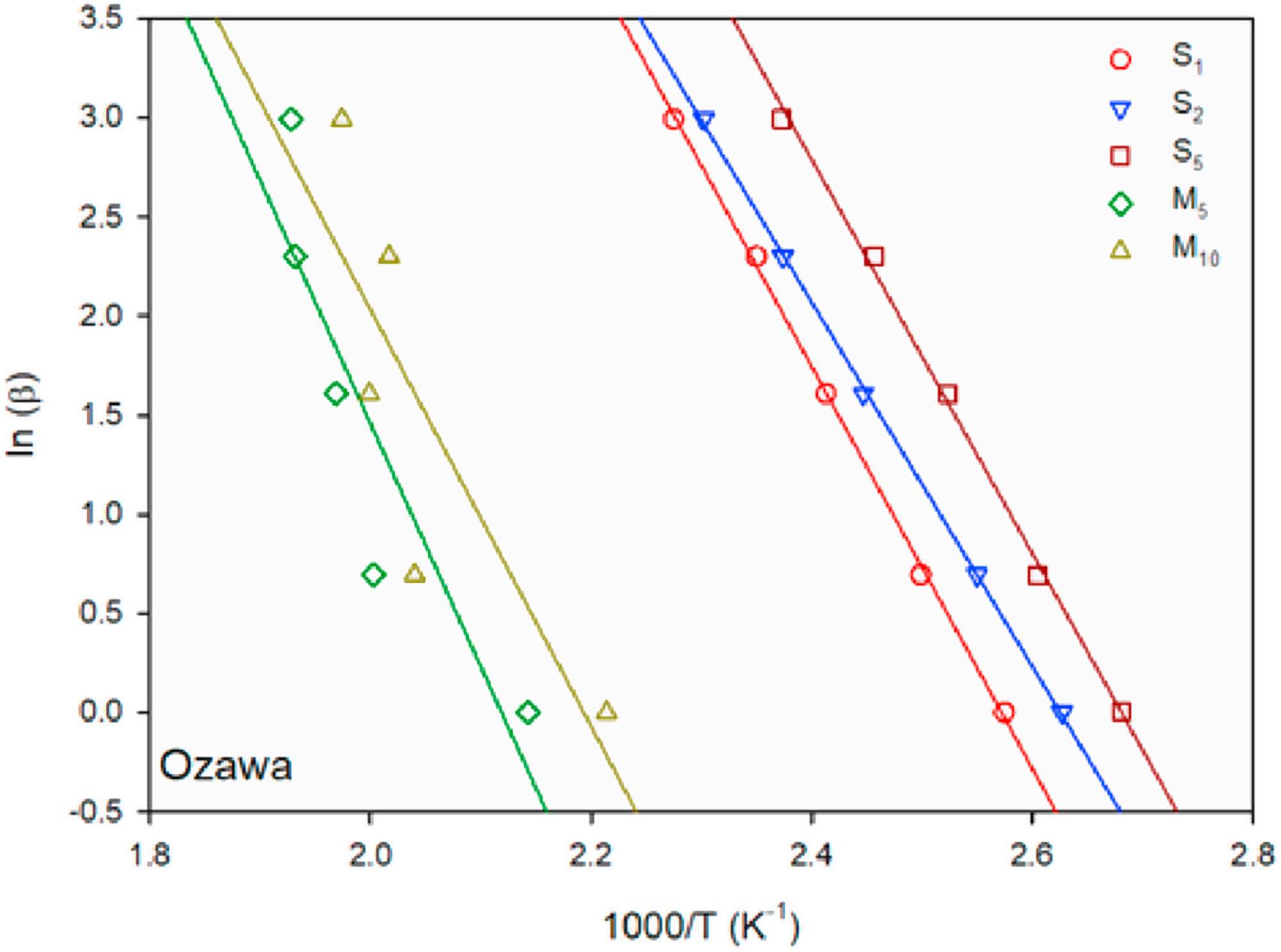
Ozawa
ln (β)
1000/T (K^{-1})
3.5
3.0
2.5
2.0
1.5
1.0
0.5
0.0
-0.5
1.8
2.0
2.2
2.4
2.6
2.8
S$_1$
S$_2$
S$_5$
M$_5$
M$_{10}$

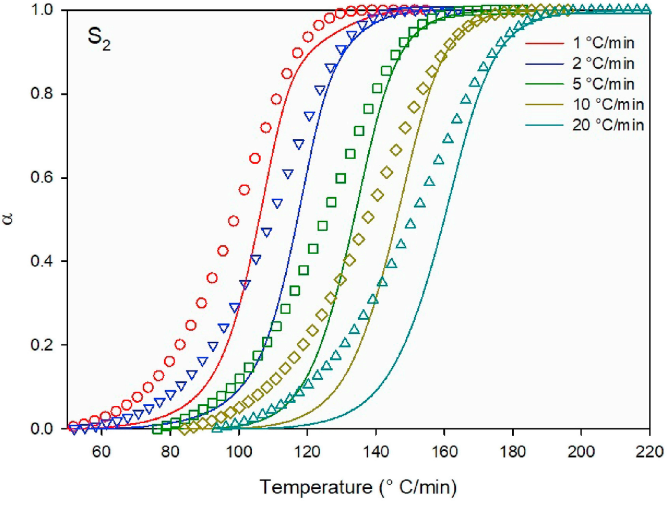
S2
1 °C/min
2 °C/min
5 °C/min
10 °C/min
20 °C/min
α
Temperature (° C/min)
0.0
0.2
0.4
0.6
0.8
1.0
60
80
100
120
140
160
180
200
220

(a)

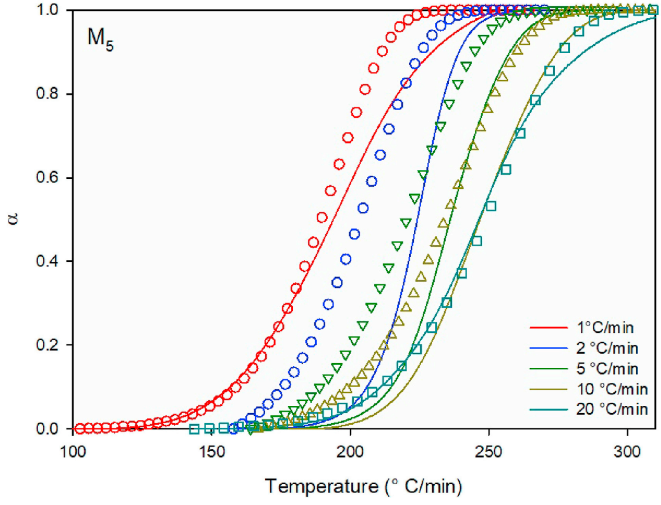
M5
1°C/min
2 °C/min
5 °C/min
10 °C/min
20 °C/min
α
Temperature (° C/min)
0.0
0.2
0.4
0.6
0.8
1.0
100
150
200
250
300

(b)

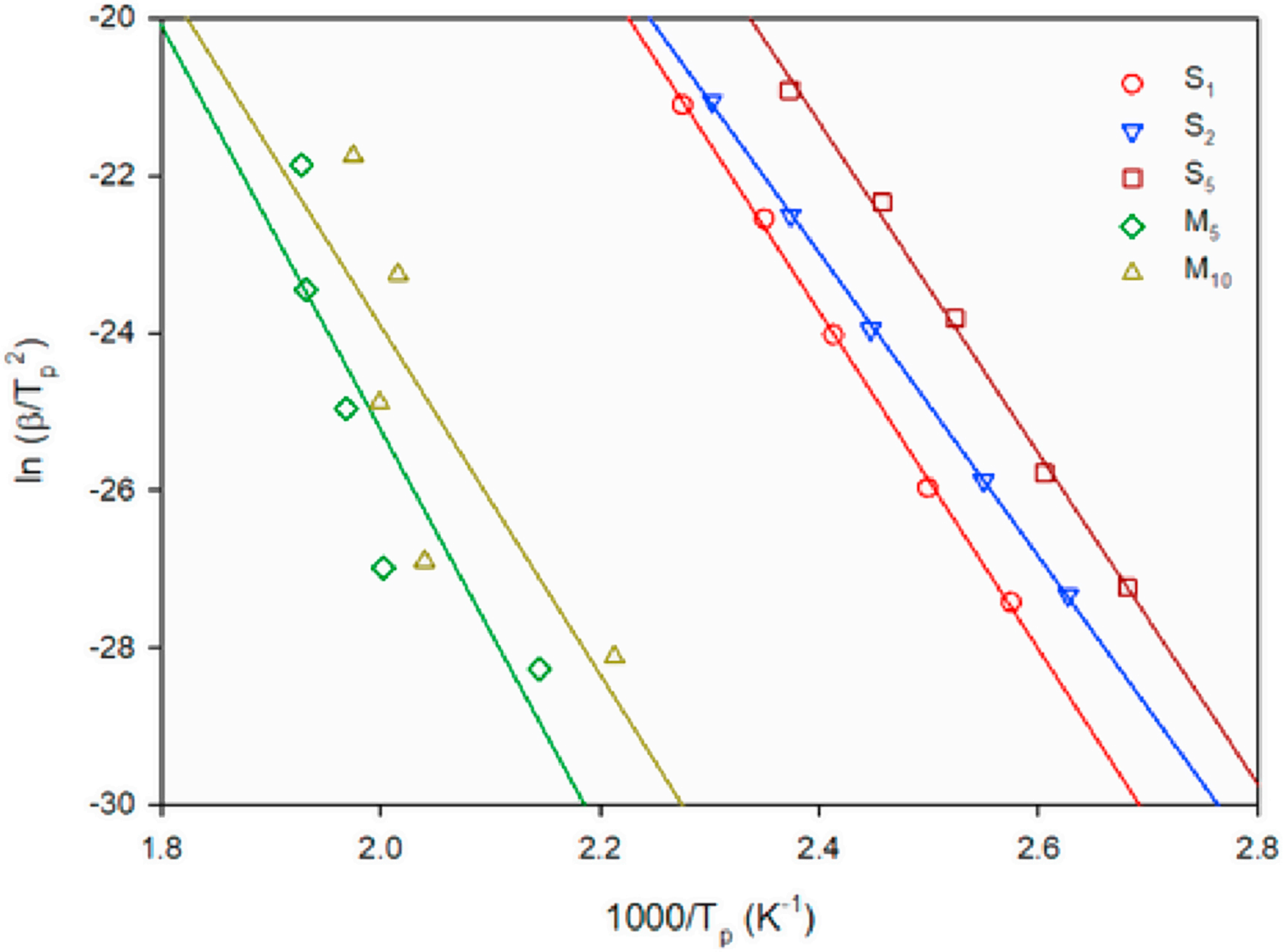
-20
-22
-24
-26
-28
-30
1.8
2.0
2.2
2.4
2.6
2.8
ln (β/T$_p^2$)
1000/T$_p$ (K^{-1})
S$_1$
S$_2$
S$_5$
M$_5$
M$_{10}$

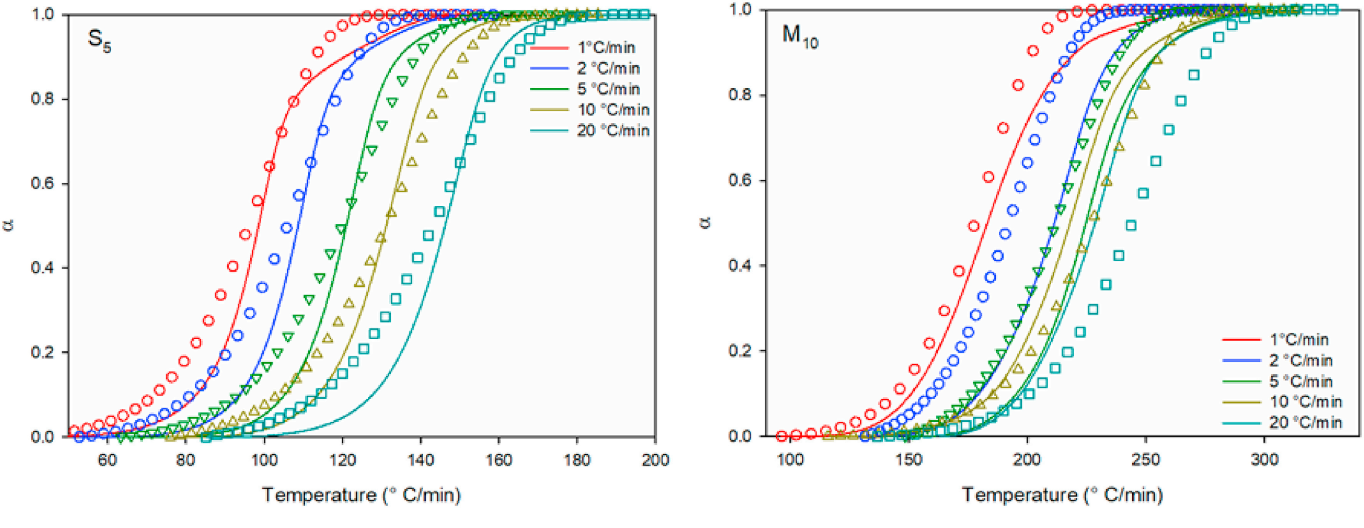
S5
1°C/min
2 °C/min
5 °C/min
10 °C/min
20 °C/min
α
Temperature (° C/min)
M10
1°C/min
2 °C/min
5 °C/min
10 °C/min
20 °C/min
α
Temperature (° C/min)

(a) (b)

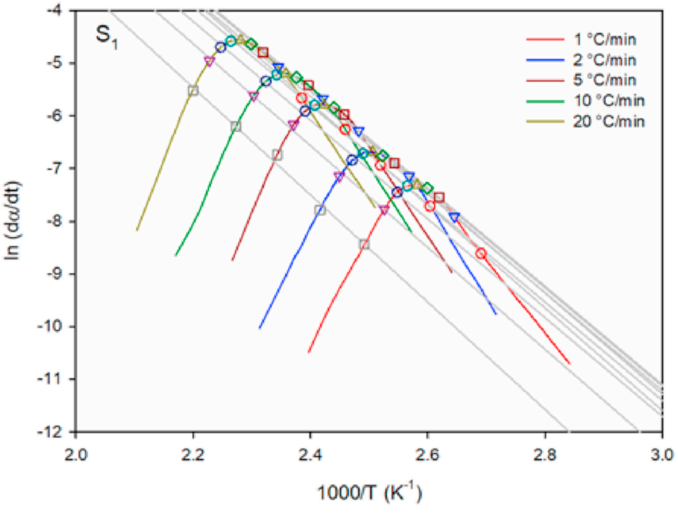
S1
1 °C/min
2 °C/min
5 °C/min
10 °C/min
20 °C/min
ln (dα/dt)
1000/T (K-1)
-4
-5
-6
-7
-8
-9
-10
-11
-12
2.0
2.2
2.4
2.6
2.8
3.0

(a)

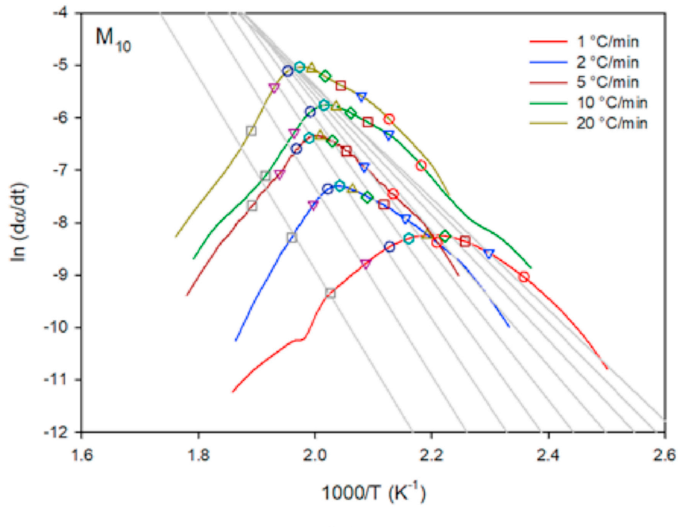
M10
1 °C/min
2 °C/min
5 °C/min
10 °C/min
20 °C/min
ln (dα/dt)
1000/T (K-1)
-4
-5
-6
-7
-8
-9
-10
-11
-12
1.6
1.8
2.0
2.2
2.4
2.6

(b)